contribution of NK alteration caused by HCV infection to the impairment of cellular immune response, which might result in chronic disease.

Materials and methods

Patients and samples. Peripheral blood (PB) samples were collected from 29 chronic HCV-infected patients attending the Department of Gastroenterology and Hepatology, Kumamoto University Hospital, Kumamoto, Japan. No patients were receiving anti-viral treatment when enrolled in the study. All 29 patients were biopsied before starting the treatment course. Out of 29 patients, 12 were followed up after starting pegylated IFN-α and ribavirin treatment. These 12 patients were followed up by sample collection and analysis at the end of treatment, and 6 months after finishing the treatment. Twenty-two age-matched healthy subjects were attending Kumamoto City Medical Association Health Care Center (Supplementary Table 1). All samples were collected with written informed consent, and the study was approved by the Ethics Committee of Kumamoto University Graduate School of Medical Science (Approval No. 657, issued 10 May, 2007).

Viral genotyping, viral load measurements, and treatment course. HCV RNA was quantified using The COBAS TaqMan HCV Test v2.0 (Roche Diagnostics, Indianapolis, IN). The detection level was 0.2 KIU/ml. The test was carried out before starting treatment, at the end of treatment, and 24 weeks after finishing treatment. Genotyping was performed using the HCV genotype primer kit from Bio Medical Laboratories (BML, Japan). Patients received Peg-IFN-α2a (Chugai Pharmaceutical, Japan) at 180 μg/week; Peg-IFN-α2b (Schering-Plough, Japan) at a weekly dose ranging 60–150 μg, and ribavirin (Roche, Schering-Plough) at a daily dose ranging 600–1000 mg/day, depending on body weight, for a period ranging 24–72 weeks (depending on HCV genotype or viral load).

Cell separation and culture stimulation. Peripheral blood mononuclear cells (PBMCs) were separated by lymphocyte separation medium (LSM Cappel, Aurora, OH) from heparinized fresh peripheral blood samples. The K562 cell line was obtained from RIKEN Cell Bank (Tsukuba, Japan), and cultured in RPMI 1640 medium (Sigma, St. Louis, MO) supplemented with 10% FBS. The effector:target cell ratio was adjusted to 10:1. Cells were suspended in RPMI and incubated in a 5% CO_2 incubator for 1 h, after which BrefeldinA (10 μg/ml) was added to detect intracellular IFN-γ, or Monensin (6 μg/ml, Sigma) was added to prevent the degradation of re-internalized CD107a (degranulation marker) proteins from the surface [17]. The cells were then incubated for a further 5 h.

Flow cytometry. The following mAbs were used in the study: CD3-PECy7 (UCHT1) and anti-Perforin (PFN)-FITC (dG9) from e-Bioscience (San Diego, CA); CD56-APC (NKH-1), NKG2D-PE (ON72), NKG2A-PE (Z199), NKp30-PE (Z25), and NKp46-PE (BAB281) from Beckman Coulter (Paris, France); CD16-Pacific Blue (3G8) from Biolegend (San Diego, CA); CD94-FITC (HP3D9), CD107a-PE (H4A3), and anti-IFN-γ FITC (4S.B3) from BD Pharmingen (San Diego, CA). For surface staining, cells were stained and incubated for 30 min on ice in the dark. For intracellular staining, cells were then washed in FACS washing medium (PBS, 0.1% NaN_3, and 3% FCS) fixed with 4% paraformaldehyde washed and permeabilized using 0.1% Saponin (Sigma), and then stained with mAbs. Cells were re-suspended in FACS washing medium and analyzed by LSRII (BD Bioscience, San Jose, CA) and FlowJo software (Tree Star, San Carlos, CA).

Statistical analysis. Graphpad Prism 5 (Graphpad Software, Inc.) was used to calculate non-parametric Mann–Whitney test to compare Patients before treatment to the control group. Paired *t*-test was used to calculate the modifications that occurred between stages in the same patient.

Results

HCV infection reduces NK cell frequency and induces shifting among its subsets

We first analyzed total NK cell number and subset frequency in PBMC of HCV-infected patients without treatment (Fig. 1A). Both the percentage and absolute number (Fig. 1B and C) of NK cells were significantly decreased in HCV patients compared to normal controls (percentage: $P = 0.0005$. Absolute number: $P = 0.0002$). Within the NK pool, the $CD56^{bright}$ subset percentage was significantly higher among HCV-infected patients ($P = 0.007$), but not the absolute number. The $CD56^{dim}16^{+}$ subset showed significant decrease among HCV patients both in percentage ($P = 0.0001$), and absolute number ($P < 0.0001$). As for the $CD56^{dim}16^{-}$ subset, also known as the activated NK subset [18,19], the percentage significantly increased in HCV patients ($P < 0.0001$) as well as the absolute number ($P = 0.03$). The $CD56^{-}16^{+}$ subset showed a significant rise among HCV-infected patients in percentage ($P = 0.02$), but not in absolute number. There were no significant correlations with viral load, genotype, AST/ALT levels, and degree of activity or liver fibrosis (data not shown). These results show that HCV affects mainly the $CD56^{dim}16^{+}$ subset, causing its decrease, leading to disruption in other subset percentages.

NCRs' and C-lectin-type receptor expression by NK cells in HCV infection

Next, we analyzed the expressions of NCRs (NKp30 and NKp46), inhibitory receptors (CD94 and NKG2A), and activation receptor NKG2D. Overall, total NK cells showed no significant difference in any of these receptors percentages (Supplementary Fig. 1A), except for NKG2D, which showed significant downregulation during HCV infection ($P < 0.0001$) (Fig. 2A and B). Detailed analysis of NK subsets showed downregulation of all NCRs by $CD56^{dim}16^{-}$ subset (Supplementary Fig. 1B).

HCV infection suppresses PFN and IFN-γ by NK cells, but degranulation ability is maintained

Cytotoxic function of NK cells depends on intracellular functional molecules, so we analyzed Perforin expression in NK cells. As shown in Fig. 2A, HCV infection significantly downregulated PFN expression by total NK cells ($P < 0.0001$). NK subset analysis (Fig. 2B) revealed that this downregulation is confined only to the $CD56^{dim}16^{+}$ subset ($P = 0.0006$). CD107a is a degranulation marker that is equivalent to cytotoxic function [17]. NK cell degranulation was significantly higher among HCV patients (Fig. 2C, $P = 0.002$). Next, we analyzed IFN-γ expression by NK cells stimulated with K562 cells. HCV infection markedly suppressed IFN-γ upregulation (Fig. 2C) ($P = 0.001$). The positive CD107a and IFN-γ subset was found to be $CD56^{dim}16^{-}$ (data not shown). The correlation between CD107a and IFN-γ expressions by the $CD56^{dim}16^{-}$ subset in normal controls was statistically significant ($r = 0.6$, $P = 0.002$), while this correlation was lost in HCV-infected subjects ($r = 0.1$, $P = 0.4$).

Pegylated IFN-α treatment modification of NK cells

We followed up 12 patients until 24 weeks after finishing the treatment course. Samples were collected from these 12 patients before starting treatment (Pre-Tx), at the end of treatment (Tx-End), when 12 subjects were negative for HCV RNA, and 24 weeks after finishing treatment (Post-Tx), when three subjects relapsed to HCV RNA positive. NK percentage did not change

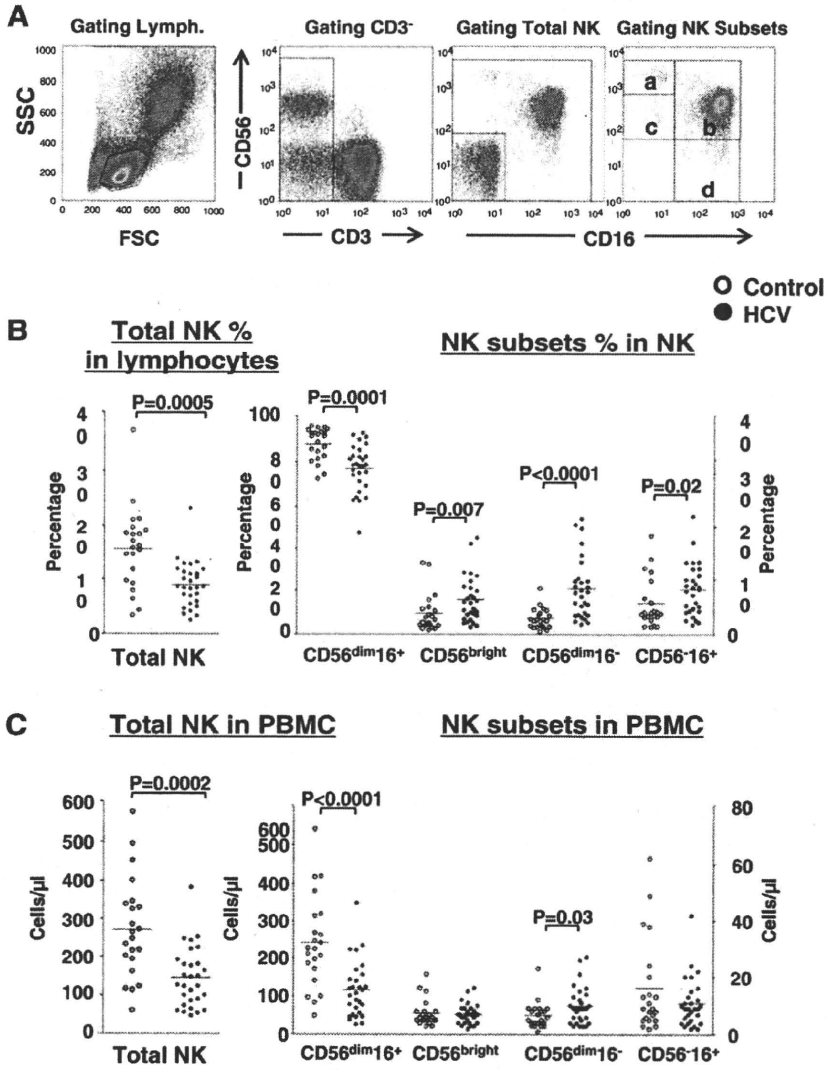

Fig. 1. Frequency and absolute number of NK cells in chronic HCV patients. (A) Lymphocytes were gated through SSC and FSC, followed by gating of $CD3^-$ events, and gating of $CD56^+$ and/or $CD16^+$ events. NK subsets were then gated on CD56 versus CD16. The plot shows the gating of (a) $CD56^{bright}$ subset, (b) $CD56^{dim}16^+$ subset, (c) $CD56^{dim}16^-$, and (d) $CD56^-16^+$ subset. (B) Total NK cell (left) percentage in lymphocytes and the 4 mentioned subset percentages (right) in NK compartment. (C) Absolute NK cell count. In panels (B) and (C), $CD56^{dim}16^+$ is plotted against the left *Y* axis, while the other subsets are plotted against the right *Y* axis. Plots show the results in healthy controls ($n = 22$) (open circles) and chronic HCV-infected subjects ($n = 29$) (closed circles). All figures show the means ± SD.

significantly throughout the follow-up period; however, the absolute numbers of NK cells (Fig. 3A) increased significantly ($P = 0.04$). The $CD56^{bright}$ (Fig. 3B) percentage increased significantly from Pre-Tx to Tx-End and decreased significantly again from Tx-End to Post-Tx ($P = 0.001$ and $P = 0.0002$, respectively). $CD56^{dim}16^+$ (Fig. 3C) showed a significant increase from Tx-End to Post-Tx both in percentage and absolute number ($P = 0.0003$, 0.02, respectively). $CD56^{dim}16^-$ (Fig. 3D) percentage decreased significantly from Tx-End to Post-Tx ($P = 0.02$), but not in absolute value. The $CD56^-16^+$ subset showed a significant decrease from patients to Tx-End in percentage, but not in absolute value ($P = 0.04$). These results show that treatment directly affects the NK cell compartment through expansion of the $CD56^{dim}16^+$ subset, resulting in the return of other NK subsets to normal by 6 months after treatment.

Anti-viral treatment recovered NK function

NKG2D (Fig. 4A) expression showed a significant increase in percentage only from Pre-Tx to Post-Tx ($P = 0.001$). PFN expression was raised significantly from Pre-Tx to Post-Tx ($P = 0.002$) (Fig. 4B), showing that anti-viral treatment upregulates PFN expression by NK cells. Although the percentage of CD107a expression decreased upon treatment, since all NK cell are increased, CD107a-expressing cells did not show any significant change in absolute cell count throughout the treatment course, or 24 weeks later (data not shown). The IFN-γ-expressing NK cell percentage rose significantly from Pre-Tx to Post-Tx ($P = 0.01$) (Fig. 4D).

Absence of NK treatment modifications in relapsed patients

Three cases relapsed to positive HCV RNA 24 weeks after treatment. Although the case number does not enable statistical analysis, the pattern of results seen in relapsed cases suggests a specific tendency. The results showed NK frequency reduction to Pre-Tx levels as well as subset distribution and PFN expression (Supplementary Fig. 2A, B, and C).

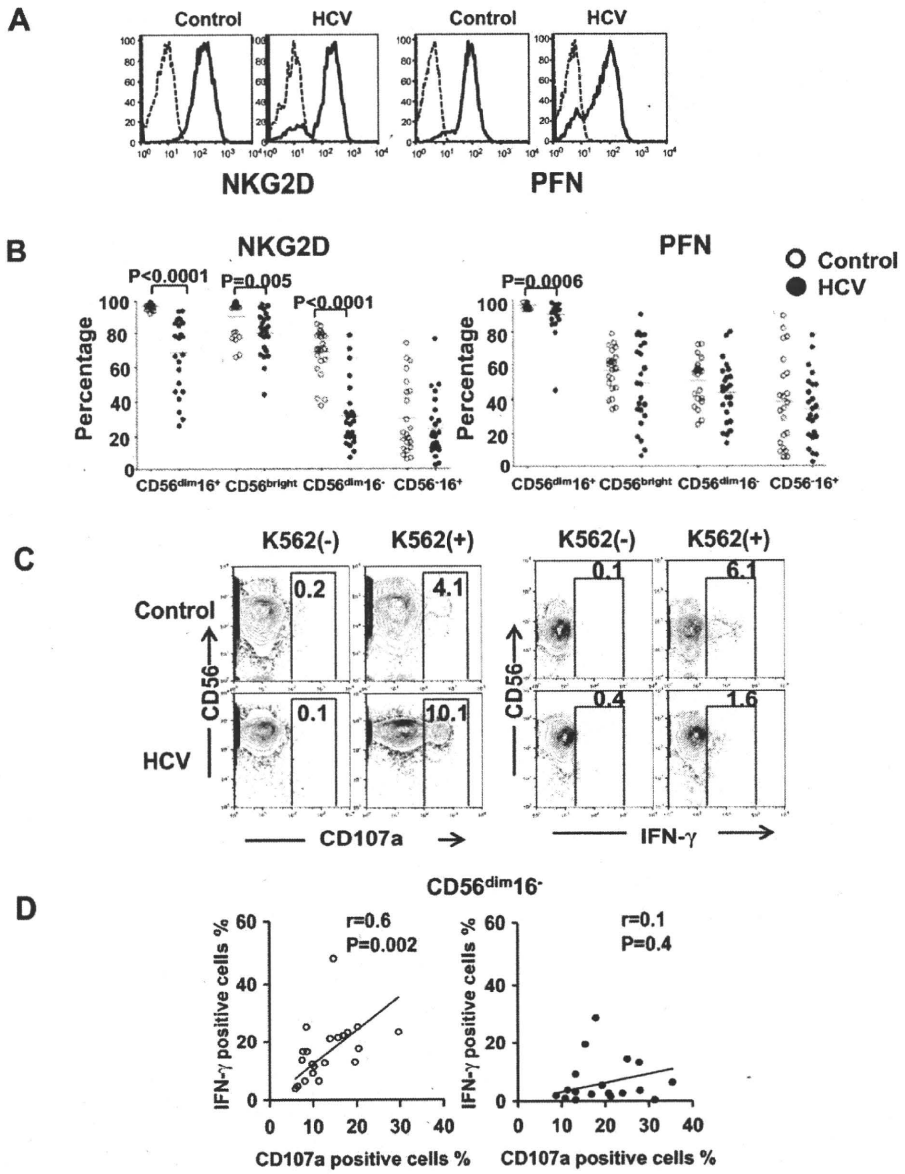

Fig. 2. Expression of NKG2D, PFN, CD107a degranulation marker and IFN-γ by NK cells in chronic HCV patients. (A) Histogram showing the expression of NKG2D and PFN in healthy control and HCV-infected patients NK cells. Isotype control is shown in dotted line. (B) Vertical scatter showing the percentage of NKG2D and PFN positive NK cells in different NK subsets in controls and HCV patients. Control: open circles, HCV patients: closed circles. (C) Contour plots showing Gated NK cells expression of CD107a and IFN-γ with and without stimulation using K562 cells, in control and HCV patients. Plots are displaying the positive cells percentage. (D) Scatter plots showing the correlation between CD107a and IFN-γ expression by $CD56^{dim}16^{-}$ subset in normal controls (left) and HCV patients (right).

Discussion

In this study, we investigated the alteration by chronic HCV of NK cell frequency, subset reconstitution, NK receptor expression, and NK functions, as well as the modification by anti-viral treatment. Study subjects consisted of both genotype 1 and 2. However, our data showed no significant difference between the two genotypes regarding NK frequency, receptors expression, or functions (data not shown). Our data confirm a significant reduction in NK cell frequency and quantitative imbalance of NK cell subsets in HCV-infected patients, which was reversed by anti-viral treatment. This reduction was localized to the $CD56^{dim}16^{+}$ subset. Detailed analysis revealed that the expression of NK activation receptor (NKG2D), PFN, and IFN-γ production were suppressed in chronic HCV patients. It is of interest that the expression of a degranulation marker, CD107a, was not influenced by chronic HCV infection. Follow-up study showed that the expression of these receptors was recovered in treated patients who eliminated HCV. Our results suggest that chronic HCV infection affects the recognition of target cells by NCRs and IFN-γ production of NK cells, and contributes to chronic HCV infection.

We analyzed in detail how the reduction in NK cell numbers and the shift of NK subsets may lead to functional deficits within the total NK cell population of chronic HCV patients. Our results show that HCV infection downregulated NKG2D by NK cells (Fig. 2). As both cytotoxicity and IFN-γ production are regulated by NKG2D-DAP10 signaling, it is reasonable that the expressions of CD107a and IFN-γ are positively correlated in normal

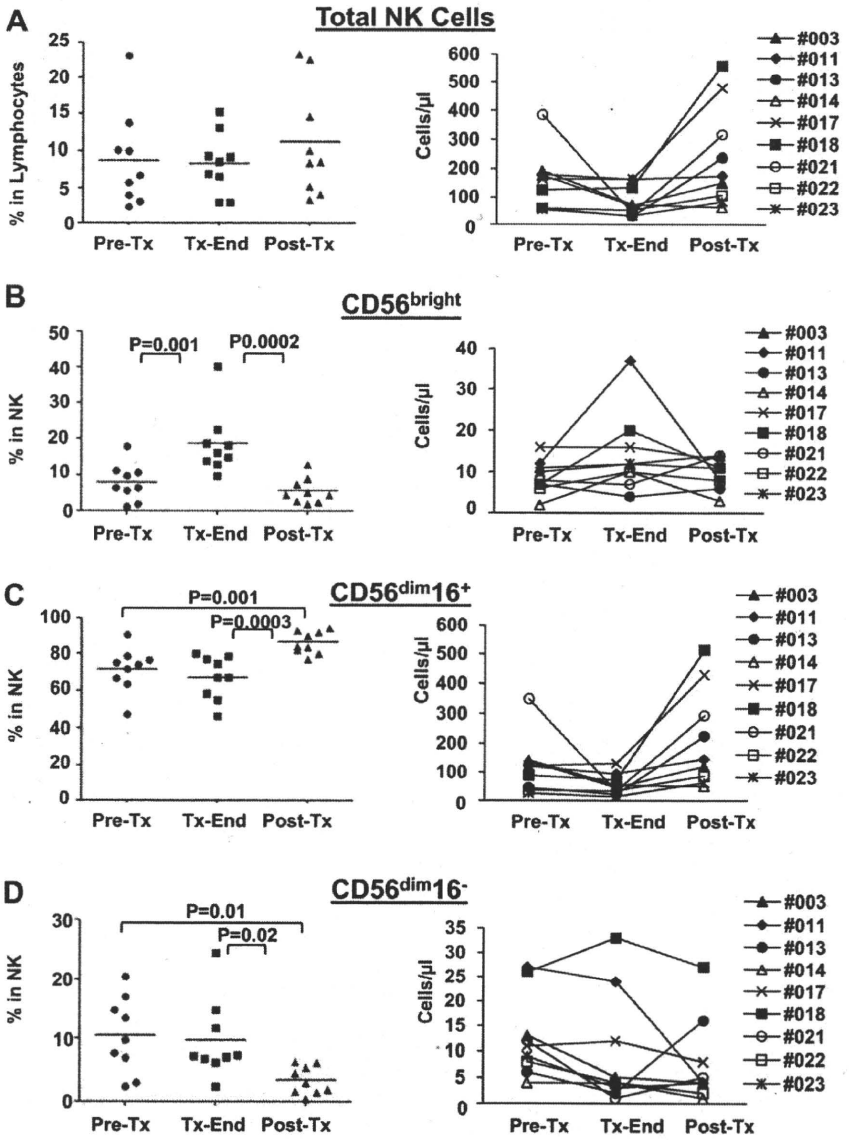

Fig. 3. Recovery of NK cell numbers and component by anti-viral treatment. Anti-viral treatment reverses the reduction in NK cell count. Vertical scatter plot showing the modification in percentage and cell count before (Pre-Tx) (closed circles), at the end (Tx-End) (closed squares), and 6 months (Post-Tx) (closed triangles) after finishing treatment in (A) total NK, (B) $CD56^{bright}$ subset, (C) $CD56^{dim}16^{+}$ subset, and (D) $CD56^{dim}16^{-}$ subset ($n = 9$).

individuals; however, it is of interest that CD107a expression upon stimulation remained high (data not shown) although NKG2D and IFN-γ expressions were suppressed in HCV patients. Since NK cell activity is regulated by the fine balance of the activating signal via NKG2D and inhibitory signals via CD94/NKG2A, modulation of the interplay between inhibitory and activation signals by HCV can markedly change the properties of NK cell function [9,20].

We followed the NK cell status of the patients before and after pegylated IFN-α and ribavirin treatment, and assessed the treatment results and status of NK cells 24 weeks after treatment. Nine of 12 patients succeeded in eliminating HCV. Overall NK cell levels, the subpopulation of NK cells, expression of NK cell receptors, and function of NK cells (CD107a and IFN-γ expressions after co-culture with K562) were recovered to normal levels. In contrast, patients relapsing after 24 weeks had not recovered these parameters. These results indicate that HCV activity affects NK cell numbers and function; however, HCV virions did not affect NK cell activation or effector function either directly or indirectly in vitro [21], indicating that HCV virions do not modulate NK function in the acute phase of infection. As regards chronic HCV infection, there are multiple reports that NK cell function is altered by HCV infection [22,23]. HCV-E2 glycoprotein is known to bind to the tetraspanin CD81 expressed by NK cells and inhibits NK cell activation and IFN-γ production [5]. In addition, HCV NS3/4A protease has been shown to interfere with IFN induction by preventing the RIG-1 helicase pathway [24] as well as IRF3 phosphorylation [25], which favors viral propagation and presumably HCV chronic infection. Elucidation of these mechanisms may lead to NK cell-mediated therapy against HCV.

In this study, we were able to exclude the individual variation in NK function and frequency, which caused the controversy in previous reports. We expected that the NK subset and function may differ between treatment responders and relapsing patients at the end of treatment, from which we can predict therapeutic performance; however, we found no relation between them at the end of treatment. This may be because the influence of administrated

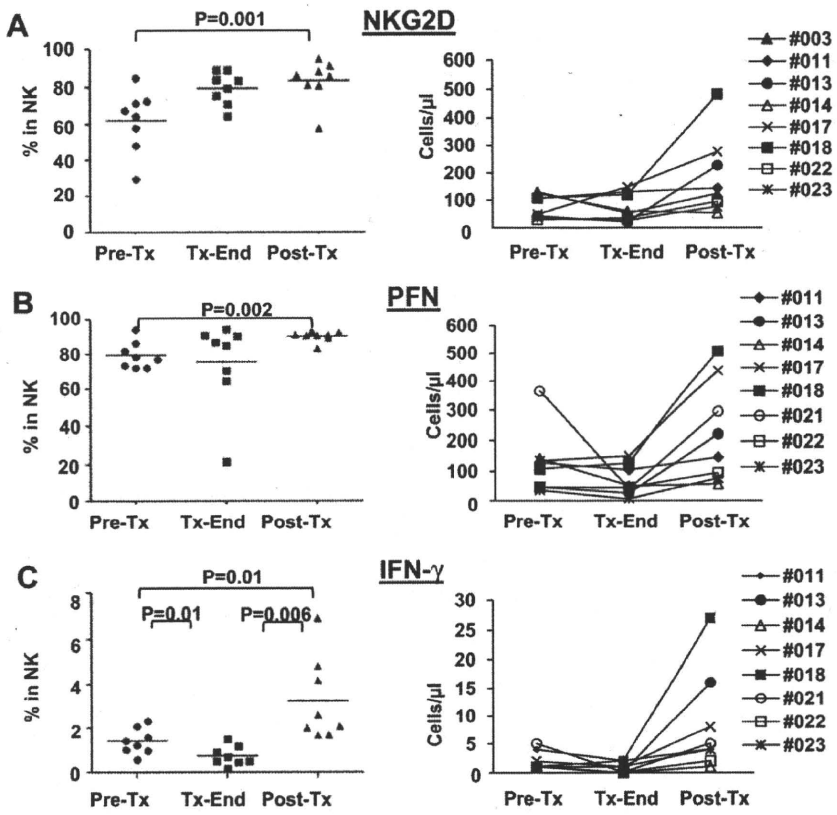

Fig. 4. Recovery of NK cell functional markers by anti-viral treatment. Vertical scatter plots for (A) NKG2D ($n = 8$), (B) PFN ($n = 8$), and (C) IFN-γ ($n = 8$) expressing NK cell percentage and cell count in patients before (Pre-Tx) (closed circles), at the end (Tx-End) (closed squares), and 6 months (Post-Tx) (closed triangles) after finishing treatment (left).

IFN-α was persisting. It is possible that recovered NK cells suppress the recurrence of HCV, since NK cells have anti-HCV activity [6]. Further detailed follow-up studies are expected to show phenotypical and functional differences between responders and non-responders, and if non-responders or early relapse can be predicted by changes in the NK cell fraction in advance, it will be a strong benefit for HCV patients.

Several studies suggest that HCV viral persistence may be associated with decreased NK cell numbers and defective NK cell responses. The reason for the decreased frequency of NK cells in chronic HCV patients is currently unknown, although possible explanations may include death or turnover, or decreased production of NK cells [23]. In addition, as cross-linking of HCV-E2 glycoprotein to CD81 inhibits the activation and proliferation of NK cells [5], it remains possible that high local concentration of envelope protein of HCV may alter NK cell function and frequency. NK cell development, maturation and function are strongly influenced by immunoregulatory cytokines, such as IL-2, IL-12, IL-15, IL-18, and IL-21, among which, Meier et al. showed that serum levels of IL-15 were significantly reduced in HCV patients and that IL-15 rescued NK cells of HCV patients from apoptosis and promoted proliferation and NK cell function ex vivo [26]. In addition, IFN-αβ is known to upregulate IL-15 production in HCV patients, and the serum level of IL-15 is significantly higher in early virological responders, whereas late virological responders show a low IL-15 level. Thus, reduced serum levels of IL-15 may also contribute to a common mechanism underlying NK cell abnormalities in HCV patients and IL-15 treatment may be beneficial for the eradication of HCV.

Conclusions

In conclusion, our study revealed that HCV chronically infected patients show conserved cytotoxic activity and dysfunctional cytokine production, which are likely due to the direct effects of HCV and may be key factors contributing to the virus persistence of chronic hepatitis. Cytokine treatment, such as IL-12, IL-15 and IL-21, may recover IFN-γ production by NK cells and support the effects of pegylated IFN-α and ribavirin treatment. Such study will be useful for the development of selective and effective therapies for chronic hepatitis C infection.

Acknowledgments

We are grateful to Ms. Yuka Hirota and Ms. Naomi Nakamichi for laboratory technical assistance and Ms. Yuka Endo and Ms. Kyoko Tokunaga for secretarial assistance. This work was supported in part by Health and Labour Sciences Research Grants from The Ministry of Health, Labour and Welfare of Japan.

Appendix A. Supplementary data

Supplementary data associated with this article can be found, in the online version, at doi:10.1016/j.bbrc.2010.02.008.

References

[1] J.G. McHutchison, Understanding hepatitis C, Am. J. Manag. Care 10 (2004) S21–S29.

[2] J.H. Hoofnagle, Course and outcome of hepatitis C, Hepatology 36 (2002) S21–S29.
[3] C.A. Biron, Activation and function of natural killer cell responses during viral infections, Curr. Opin. Immunol. 9 (1997) 24–34.
[4] S. Crotta, A. Stilla, A. Wack, A. D'Andrea, S. Nuti, U. D'Oro, M. Mosca, F. Filliponi, R.M. Brunetto, F. Bonino, S. Abrignani, N.M. Valiante, Inhibition of natural killer cells through engagement of CD81 by the major hepatitis C virus envelope protein, J. Exp. Med. 195 (2002) 35–41.
[5] C.T. Tseng, G.R. Klimpel, Binding of the hepatitis C virus envelope protein E2 to CD81 inhibits natural killer cell functions, J. Exp. Med. 195 (2002) 43–49.
[6] Y. Li, T. Zhang, C. Ho, J.S. Orange, S.D. Douglas, W.Z. Ho, Natural killer cells inhibit hepatitis C virus expression, J. Leukoc. Biol. 76 (2004) 1171–1179.
[7] V.D. Gonzalez, K. Falconer, J. Michaelsson, M. Moll, O. Reichard, A. Alaeus, J.K. Sandberg, Expansion of CD56– NK cells in chronic HCV/HIV-1 co-infection: reversion by antiviral treatment with pegylated IFNalpha and ribavirin, Clin. Immunol. 128 (2008) 46–56.
[8] S. Norris, C. Collins, D.G. Doherty, F. Smith, G. McEntee, O. Traynor, N. Nolan, J. Hegarty, C. O'Farrelly, Resident human hepatic lymphocytes are phenotypically different from circulating lymphocytes, J. Hepatol. 28 (1998) 84–90.
[9] P. Bonorino, M. Ramzan, X. Camous, T. Dufeu-Duchesne, M.A. Thelu, N. Sturm, A. Dariz, C. Guillermet, M. Pernollet, J.P. Zarski, P.N. Marche, V. Leroy, E. Jouvin-Marche, Fine characterization of intrahepatic NK cells expressing natural killer receptors in chronic hepatitis B and C, J. Hepatol. 51 (2009) 458–467.
[10] G. Ahlenstiel, R.H. Titerence, C. Koh, B. Edlich, J.J. Feld, Y. Rotman, M.G. Ghany, J.H. Hoofnagle, T.J. Liang, T. Heller, B. Rehermann, Natural killer cells are polarized toward cytotoxicity in chronic hepatitis C in an interferon-alfa-dependent manner, Gastroenterology 138 (2010) 325–335.
[11] M.W. Fried, M.L. Shiffman, K.R. Reddy, C. Smith, G. Marinos, F.L. Goncales Jr., D. Haussinger, M. Diago, G. Carosi, D. Dhumeaux, A. Craxi, A. Lin, J. Hoffman, J. Yu, Peginterferon alfa-2a plus ribavirin for chronic hepatitis C virus infection, N. Engl. J. Med. 347 (2002) 975–982.
[12] S.J. Hadziyannis, H. Sette Jr., T.R. Morgan, V. Balan, M. Diago, P. Marcellin, G. Ramadori, H. Bodenheimer Jr., D. Bernstein, M. Rizzetto, S. Zeuzem, P.J. Pockros, A. Lin, A.M. Ackrill, Peginterferon-alpha2a and ribavirin combination therapy in chronic hepatitis C: a randomized study of treatment duration and ribavirin dose, Ann. Intern. Med. 140 (2004) 346–355.
[13] G.C. Sen, Viruses and interferons, Annu. Rev. Microbiol. 55 (2001) 255–281.
[14] H. Tilg, New insights into the mechanisms of interferon alfa: an immunoregulatory and anti-inflammatory cytokine, Gastroenterology 112 (1997) 1017–1021.
[15] F. Lechner, D.K. Wong, P.R. Dunbar, R. Chapman, R.T. Chung, P. Dohrenwend, G. Robbins, R. Phillips, P. Klenerman, B.D. Walker, Analysis of successful immune responses in persons infected with hepatitis C virus, J. Exp. Med. 191 (2000) 1499–1512.
[16] S.H. Wang, C.X. Huang, L. Ye, X. Wang, L. Song, Y.J. Wang, H. Liang, X.Y. Huang, W.Z. Ho, Natural killer cells suppress full cycle HCV infection of human hepatocytes, J. Viral Hepat. 15 (2008) 855–864.
[17] G. Alter, J.M. Malenfant, M. Altfeld, CD107a as a functional marker for the identification of natural killer cell activity, J. Immunol. Methods 294 (2004) 15–22.
[18] O. Penack, C. Gentilini, L. Fischer, A.M. Asemissen, C. Scheibenbogen, E. Thiel, L. Uharek, CD56dimCD16neg cells are responsible for natural cytotoxicity against tumor targets, Leukemia 19 (2005) 835–840.
[19] B. Grzywacz, N. Kataria, M.R. Verneris, CD56(dim)CD16(+) NK cells downregulate CD16 following target cell induced activation of matrix metalloproteinases, Leukemia 21 (2007) 356–359. author reply 359.
[20] J. Nattermann, G. Feldmann, G. Ahlenstiel, B. Langhans, T. Sauerbruch, U. Spengler, Surface expression and cytolytic function of natural killer cell receptors is altered in chronic hepatitis C, Gut 55 (2006) 869–877.
[21] J.C. Yoon, M. Shiina, G. Ahlenstiel, B. Rehermann, Natural killer cell function is intact after direct exposure to infectious hepatitis C virions, Hepatology 49 (2009) 12–21.
[22] A. De Maria, M. Fogli, S. Mazza, M. Basso, A. Picciotto, P. Costa, S. Congia, M.C. Mingari, L. Moretta, Increased natural cytotoxicity receptor expression and relevant IL-10 production in NK cells from chronically infected viremic HCV patients, Eur. J. Immunol. 37 (2007) 445–455.
[23] C. Morishima, D.M. Paschal, C.C. Wang, C.S. Yoshihara, B.L. Wood, A.E. Yeo, S.S. Emerson, M.C. Shuhart, D.R. Gretch, Decreased NK cell frequency in chronic hepatitis C does not affect ex vivo cytolytic killing, Hepatology 43 (2006) 573–580.
[24] E. Foy, K. Li, R. Sumpter Jr., Y.M. Loo, C.L. Johnson, C. Wang, P.M. Fish, M. Yoneyama, T. Fujita, S.M. Lemon, M. Gale Jr., Control of antiviral defenses through hepatitis C virus disruption of retinoic acid-inducible gene-I signaling, Proc. Natl. Acad. Sci. USA 102 (2005) 2986–2991.
[25] E. Foy, K. Li, C. Wang, R. Sumpter Jr., M. Ikeda, S.M. Lemon, M. Gale Jr., Regulation of interferon regulatory factor-3 by the hepatitis C virus serine protease, Science 300 (2003) 1145–1148.
[26] U.C. Meier, R.E. Owen, E. Taylor, A. Worth, N. Naoumov, C. Willberg, K. Tang, P. Newton, P. Pellegrino, I. Williams, P. Klenerman, P. Borrow, Shared alterations in NK cell frequency, phenotype, and function in chronic human immunodeficiency virus and hepatitis C virus infections, J. Virol. 79 (2005) 12365–12374.

MOLECULAR AND CELLULAR BIOLOGY, Aug. 2010, p. 3994–4005 Vol. 30, No. 16
0270-7306/10/$12.00 doi:10.1128/MCB.01358-09

The Anaphase-Promoting Complex/Cyclosome Activator Cdh1 Modulates Rho GTPase by Targeting p190 RhoGAP for Degradation▽†

Hideaki Naoe,[1,4] Kimi Araki,[3] Osamu Nagano,[1,2] Yusuke Kobayashi,[1] Jo Ishizawa,[1] Tatsuyuki Chiyoda,[1] Takatsune Shimizu,[1,2] Ken-ichi Yamamura,[3] Yutaka Sasaki,[4] Hideyuki Saya,[1,2] and Shinji Kuninaka[1]*

Division of Gene Regulation, Institute for Advanced Medical Research, Keio University School of Medicine, Tokyo 160-8582, Japan[1]; CREST, Japan Science and Technology Agency, Tokyo 102-0075, Japan[2]; and Laboratory of Developmental Genetics, Division of Organogenesis, Institute of Molecular Embryology and Genetics,[3] and Department of Gastroenterology and Hepatology, School of Medicine,[4] Kumamoto University, Kumamoto 860-8556, Japan

Received 12 October 2009/Returned for modification 30 November 2009/Accepted 24 May 2010

Cdh1 is an activator of the anaphase-promoting complex/cyclosome and contributes to mitotic exit and G_1 maintenance by targeting cell cycle proteins for degradation. However, Cdh1 is expressed and active in postmitotic or quiescent cells, suggesting that it has functions other than cell cycle control. Here, we found that homozygous *Cdh1* gene-trapped (*Cdh1*$^{GT/GT}$) mouse embryonic fibroblasts (MEFs) and *Cdh1*-depleted HeLa cells reduced stress fiber formation significantly. The GTP-bound active Rho protein was apparently decreased in the *Cdh1*-depleted cells. The p190 protein, a major GTPase-activating protein for Rho, accumulated both in *Cdh1*$^{GT/GT}$ MEFs and in *Cdh1*-knockdown HeLa cells. Cdh1 formed a physical complex with p190 and stimulated the efficient ubiquitination of p190, both in *in vitro* and *in vivo*. The motility of *Cdh1*-depleted HeLa cells was impaired; however, codepletion of p190 rescued the migration activity of these cells. Moreover, *Cdh1*$^{GT/GT}$ embryos exhibited phenotypes similar to those observed for Rho-associated kinase I and II knockout mice: eyelid closure delay and disruptive architecture with frequent thrombus formation in the placental labyrinth layer, respectively. Furthermore, the p190 protein accumulated in the *Cdh1*$^{GT/GT}$ embryonic tissues. Our data revealed a novel function for Cdh1 as a regulator of Rho and provided insights into the role of Cdh1 in cell cytoskeleton organization and cell motility.

The anaphase-promoting complex/cyclosome (APC/C) is a multisubunit complex that functions as an E3 ubiquitin ligase for various cell cycle proteins (19, 46). Proteins ubiquitinated by APC/C are recognized and degraded by the 26S proteasome to ensure proper cell cycle progression. APC/C activity is strictly dependent on coactivator proteins that interact with APC/C during specific phases of the cell cycle. Cdh1 (also known as Fzr, Hct1, or Srw) is one of the coactivators that maintain APC/C activity from anaphase of mitosis until the end of the G_1 phase of the cell cycle (43, 53).

The role of Cdh1 (APC/C^{Cdh1}) on cell-cycle progression has been well studied; however, several studies have shed light into another aspect of Cdh1's function. For example, expression of Cdh1 is not restricted to cycling cells; APC/C^{Cdh1} is also present and active in quiescent cultured cells (9). Furthermore, immunohistochemical analysis has shown that Cdh1 is expressed in a wide variety of tissues that are predominantly composed of postmitotic cells, such as neurons, where APC/C^{Cdh1} has a high cyclin B ubiquitination activity (1, 16). It has been reported that APC/C^{Cdh1} promotes axonal growth and patterning (20) and is required for neuronal survival (1). These results highlight the importance of the APC/C activator Cdh1 in neurons. However, Cdh1 has also been shown to participate in the differentiation of tissues such as the muscle (25). Given that Cdh1 is ubiquitously expressed in organs containing quiescent cells, there might be additional roles for Cdh1.

Rho GTPase proteins play a central role in the regulation of cell shape, polarity, and locomotion via their effects on actin polymerization, actomyosin contractility, cell adhesion, and microtubule dynamics (13). Small G proteins, which include Rho, act as molecular switches that cycle between an inactive GDP-bound state and an active GTP-bound state. The latter form of Rho proteins interacts with and activates downstream effector proteins. The activity of Rho GTPases is controlled by three class of key regulators: (i) guanine nucleotide exchange factors (GEFs), which catalyze the exchange of GDP to GTP for their activation (41); (ii) GTPase activating proteins (GAPs), which stimulate the intrinsic GTPase activity for their inactivation (8); and (iii) guanine nucleotide dissociation inhibitors (GDIs), which interact with GDP-bound Rho GTPases and sequester them in the cytoplasm to inhibit the exchange of GDP to GTP (33). In addition to these canonical regulations, recent studies indicate that the ubiquitination pathway is also involved in the modulation of Rho GTPase activity. Smurf1, which is a HECT domain E3 ubiquitin ligase, controls the local levels of RhoA at the cell periphery by targeting it for degradation (40, 55). Therefore, the regulatory mechanisms of Rho GTPase activity seem to be more complex than previously thought. It thus remains to be clarified whether

* Corresponding author. Mailing address: Division of Gene Regulation, Institute for Advanced Medical Research, Keio University School of Medicine, Tokyo 160-8582, Japan. Phone: 81 3 5363 3983. Fax: 81 3 5363 3982. E-mail: skuninak@a8.keio.jp.

† Supplemental material for this article may be found at http://mcb.asm.org/.

▽ Published ahead of print on 7 June 2010.

other ubiquitin ligases also play a role in Rho signaling by targeting its components directly or indirectly.

In this study, we found that the APC/C activator Cdh1 modulated actin organization. Mouse embryonic fibroblasts (MEFs) derived from a homozygous *Cdh1* gene-trapped ([GT] $Cdh1^{GT/GT}$) mouse model displayed decreased numbers of stress fibers and focal adhesions (FAs). Consistent with these phenotypes, Rho activity was apparently reduced in *Cdh1*-deficient cells. Cdh1 regulated Rho activity via the targeting of p190 for degradation. We also found that Cdh1 knockdown cells showed decreased motility, which was rescued by codepletion of p190. Furthermore, phenotypic similarities between $Cdh1^{GT/GT}$ embryos and ROCK (also known as Rho-kinase, which is the important Rho downstream effector of actin cytoskeleton formation) knockout (KO) mice (44, 49) support our notion that Cdh1 plays a role in the Rho/ROCK signaling axis. Collectively, our findings suggest an alternative role for Cdh1 other than cell cycle regulation and reveal Cdh1 as a new regulator of Rho.

MATERIALS AND METHODS

Mice. $Cdh1^{+/GT}$ mice (C57BL/6 background) were derived from the TT2 embryonic stem (ES) cell line (57) by integration of the pU-17 exchangeable GT vector (48) into the *Cdh1* locus. These mice were obtained from TransGenic (Kumamoto, Japan). Characterization of the vector insertion site was performed by 5′ rapid amplification of cDNA ends (5′ RACE) and plasmid rescue experiments. Genotyping of the mutant mice was performed using a PCR protocol based on the primers Gs4 (5′-CCTCCACTACAGCAGCACG-3′), Gas7 (5′-CTCCAAGGCCTTTGTGAGGC-3′), and SA6as (5′-CCGGCTAAAACTTGAGACCTTC-3′) (see Fig. S1 in the supplemental material). For detection of the Cdh1–β-*geo* fusion mRNA, oligo(dT)-primed cDNAs derived from mutant mice were subjected to PCR using the primers 5NC-s (5′-TGTTCCTGGGACCGGCGGGAAC-3′) and LZUS-3 (5′-CGCATCGTAACCGTGCATCT-3′). The amplification product was cloned into the TA cloning vector and sequenced. All animal experiments were approved by the Animal Ethics Committees of Keio University and Kumamoto University.

Replacement of the β-*geo* gene cassette. To produce ES cells in which the β-*geo* gene cassette of $Cdh1^{+/GT}$ cells was replaced with the *Cdh1* cDNA, we introduced the P17/Cdh1 replacement vector (see Fig. S2C in the supplemental material) together with pCAGGS-Cre (encoding Cre recombinase) (3) into $Cdh1^{+/GT}$ ES cells using electroporation. Cells were cultured in medium containing puromycin for 1 day to isolate cell lines that had undergone recombination. Puromycin selection was performed twice at a 2-day interval. To detect the expression of the knock-in (KI) *Cdh1* ($Cdh1^{KI}$) allele, we performed reverse transcription-PCR (RT-PCR) analysis using the primers 5NC-s2 (5′-TCGAACAGGCGCGGCGTGTT-3′) and mFzr as2 (5′-ATAGTCCTGGTCCATGGTGGAG-3′) (see Fig. S2C). The PCR product was cloned into the pGEM-T easy vector (Promega) and sequenced.

Cell culture and transfection. MEFs were prepared as follows. After mating with $Cdh1^{+/GT}$ male mice, a pregnant female $Cdh1^{+/GT}$ mouse was sacrificed at 11.5 days postcoitus (dpc), and the uterus was removed and washed in phosphate-buffered saline (PBS). The yolk sacs were separated for genotyping, and the embryos were isolated and washed in PBS. The viscera of each embryo were removed under a dissecting microscope, and the embryo was washed in PBS and incubated with TrypLE Express (Invitrogen) for 20 min at 37°C. The cell suspension was then passed several times through a pipette and filtered through a sterile cell strainer (100-μm pore size) to remove cell clumps. The cell suspension prepared from each embryo was washed with medium containing 10% fetal bovine serum (FBS) and plated onto 100-mm culture dishes. MEFs were maintained in Dulbecco's modified Eagle's medium (DMEM)-F12 supplemented with 10% FBS and antibiotics. For immortalization of MEFs, primary MEFs were transfected with simian virus 40 (SV40) large T antigen, which was prepared by transfection of Plat-E cells with pWZL-hyg-SV40 large T (28). Cells were selected in medium containing hygromycin for a week. The resultant immortalized MEFs were maintained in the medium described above. The human embryonic kidney cell line HEK293T (RCB2202) was provided by the RIKEN BRC through the National Bio-Resource Project of the MEXT, Japan. Culture and transfection of HeLa and HEK293T cells were performed as described previously (23). pEGFP-c/full-length p190 (where EGFP is enhanced green fluorescent protein) was kindly provided by H. Sabe (51). Cells were subjected to transient transfection in six-well plates using Fugene HD reagent (Roche). The transfection procedures used in the RNA interference (RNAi) experiments and the small interfering RNA (siRNA) oligonucleotides for Cdh1 and the control were as described previously (23). The target sequences of other siRNAs were as follows: siEmi1, 5′-GAGAAUUUCGGUGACAGUCUA-3′ (27), and sip190, 5′-UUGACAUCGUGGAAGUGAAGA-3′.

Quantitative analysis of gene expression. Total RNA was extracted from MEFs using an RNeasy Minikit (Qiagen) and was subjected to RT using PrimeScript (Takara). Real-time PCR was performed in a Thermal Cycler Dice (Takara) using SYBR Premix Ex *Taq* (Takara). The primers used for the amplification of murine *p190* and the glyceraldehyde-3-phosphate dehydrogenase gene (*GAPDH*) were obtained from Takara. Relative mRNA levels were calculated by normalization of the cycle threshold (C_T) values of the target gene to those of the reference gene (*GAPDH*).

Immunofluorescence microscopy. MEFs or HeLa cells were seeded onto 35-mm dishes (5×10^4 cells per dish) the day before the analysis. Cells were fixed with 4% paraformaldehyde-PBS for 15 min, which was followed by permeabilization with 0.2% Triton X-100–PBS. Cells were then incubated and stained with an antipaxillin antibody. This was followed by incubation with Alexa Fluor 488-conjugated phalloidin and Alexa Fluor 555-conjugated anti-mouse antibody (Molecular Probes). The stained cells were mounted with 1,4-diazabicyclo-[2,2,2]-octane–glycerol and were examined using a confocal microscope (FV300; Olympus). Densitometric analysis of the signal of each cell labeled with Alexa Fluor 488-conjugated phalloidin was performed using MetaXpress software (Molecular Devices).

Histochemistry, immunostaining, and X-Gal (5-bromo-4-chloro-3-indolyl-β-D-galactopyranoside) staining. For histological analysis, tissues were fixed overnight with 4% paraformaldehyde in PBS, embedded in paraffin, and then sectioned and stained with hematoxylin-eosin. For immunochemistry of eyelid epithelial sheets, 4-μm sections were prepared from 18.5-dpc embryos and boiled for 20 min in citrate buffer (pH 7.0) in a microwave oven to retrieve antigens. Nonspecific sites were blocked with mouse-on-mouse (MOM; Vector Laboratories) solution in PBS for 1 h. Sections were incubated overnight with mouse anti-p190 (1:50; BD) in MOM diluent, washed three times with PBS, and incubated with biotinylated anti-mouse IgG in MOM diluent for 10 min. Staining and development were performed using Elite ABC reagent (Vector Laboratories) and diaminobenzidine (DAB) substrate (Wako). For immunostaining of whole embryos, 12.5-dpc embryos were embedded in Tissue-Tek OCT compound medium (Sakura) and frozen in acetone-dry ice. Cryosections were stained as described above.

Immunoprecipitation, Western blotting, and antibodies. Immunoprecipitation and Western blotting were performed as described previously (23) with slight modification. We used magnetic Dynal beads (Invitrogen) for immunoprecipitation instead of agarose beads. The antibodies used in this study were anti-Myc (9E10; Santa Cruz Biotechnology), 1:1,000; anti-HA (12CA5; Santa Cruz Biotechnology), 1:1,000; anti-GFP (full-length; Santa Cruz Biotechnology), 1:500; anti-Cdh1 (DH01; Abcam), 1:500; anti-p190 (BD), 1:1,000; anti-α-tubulin (B-5-1-2; Sigma), 1:50,000; anti-RhoA, -B, and -C (Cell Signaling), 1:1,000; anti-Rac1 (Upstate Biotechnology), 1:1,000; anti-RhoGDI (Millipore), 1:500; anti-Skp2 (Zymed), 1:250; anti-cyclin B (GNS1; Santa Cruz), 1:200; and anti-Emi1 (Zymed), 1:200; anti-cdc27 (AF3.1; Santa Cruz Biotechnology), 1:500; and anti-His (MBL), 1:500. For immunoprecipitation and Western blotting of Cdh1, we generated a polyclonal antibody against Cdh1 by injecting rabbits with a synthetic peptide (MDQDYERRLLRQII, corresponding to mouse Cdh1 amino acids 1 to 14) coupled to keyhole limpet-hemocyanin (KLH) via a cysteine added at the C terminus.

Rho activation assay. HEK293 cells were transfected with siRNA oligonucleotides against Cdh1 or control. After 48 h of transfection, cells were treated with lysophosphatidic acid ([LPA] 10 μM; Sigma) for 10 min before being harvested. Cells were lysed by incubation with magnesium-containing buffer (25 mM HEPES, pH 7.5, 150 mM NaCl, 1% Igepal CA-630, 10 mM $MgCl_2$, 1 mM EDTA, and 2% glycerol) supplemented with 25 mM sodium fluoride, 1 mM sodium orthovanadate, 20 μM MG132, and protease inhibitor cocktail (Roche). After centrifugation of the lysate at 14,000 × *g* for 5 min at 4°C, the resulting supernatant was incubated with 25 μg of glutathione *S*-transferase (GST)-RBD (where RBD is the Rho-binding domain of rhotekin [amino acids 7 to 89]) bound to glutathione-Sepharose beads (GE Health Care) for 30 min at 4°C. The beads were then washed three times with magnesium-containing buffer and were subjected to immunoblot analysis using an anti-RhoA, -B, and -C polyclonal antibodies (Upstate Biotechnology). Whole-cell lysates were also immunoblotted for Rho as a loading control.

***In vitro* and *in vivo* ubiquitination assays.** For production of recombinant Cdh1 protein, a mouse Cdh1 cDNA was subcloned into pFASTBAC1 (Invitrogen) with an oligonucleotide linker corresponding to a penta-His tag. Baculoviruses were prepared according to the manufacturer's instructions (Invitrogen). Sf9 cells were transfected at a multiplicity of infection (MOI) of 10 with baculovirus for 72 h. Recombinant Cdh1 proteins were purified using a Ni-nitrilotriacetic acid (NTA) spin kit (Qiagen). The *in vitro* ubiquitination assay was performed as described previously (22, 47) with slight modification. Briefly, HeLa cells were lysed in lysis buffer (0.5% NP-40, 25 mM Tris-Cl [pH 7.5], 150 mM NaCl, 1 mM $MgCl_2$, 10% glycerol, and complete protease inhibitor cocktail [EDTA free; Roche]). APC/C was immunoprecipitated from the lysates using an anti-cdc27 antibody (Santa Cruz Biotechnology). Immunopurified APC/C was bound to recombinant Cdh1 protein and was then subjected to the ubiquitination reaction. APC/C-bound antibody beads were mixed with a reaction buffer (20 mM Tri-Cl [ph7.5], 150 mM NaCl, 1 mM dithiothreitol [DTT], 10% glycerol) containing purified E1 (80 μg/ml; Biomol), UbcH10 and UbcH5a (50 μg/ml each; Wako), ubiquitin (1.25 mg/ml; Sigma), ATP regenerating system (10 mM creatine phosphate, 2 mM ATP, 1 mM $MgCl_2$, 0.1 mM EGTA, and 39 U/ml rabbit creatine phosphokinase type I), and substrate (22). Myc-tagged full-length p190 protein (which was used as a substrate) was generated by *in vitro* translation using a TNT T7 Quick Coupled Transcription/Translation System (Promega) and biotinylated lysine (Promega Transcend tRNA), according to the manufacturer's instructions. Ubiquitinated p190 was detected by using anti-p190 antibody or streptavidin-horseradish peroxidase ([HRP] Promega). For *in vivo* ubiquitination assays, 293T cells transfected with a plasmid encoding hemagglutinin (HA)-tagged human ubiquitin and pEGFP-c/full-length p190 were incubated with 10 μM MG132 for 6 h after 24 h of cell culture. Cells were collected and subjected to immunoprecipitation using an anti-GFP antibody. Samples were immunoblotted to detect polyubiquitination using an anti-HA antibody.

Cell migration assay. Cell migration was measured using a 24-well Boyden chamber (BD). HeLa cells were transfected with siRNA 48 h before the assay. Cells (5×10^4) were seeded in serum-free medium (0.5 ml) in the upper chamber, with serum-containing medium in the lower chamber. After 24 h of incubation at 37°C, nonmigrating cells in the upper chamber were scraped using a cotton swab, and the undersides of the membranes were fixed with 100% methanol and stained with 50% Giemsa solution. The migrating cells at the bottom of the filters were counted (four fields per filter) in three independent experiments.

Establishment of $Cdh1^{GT/GT}$ ES cells and tetraploid aggregation experiments. To generate $Cdh1^{GT/GT}$ ES cell lines, we cultured delayed two-cell-stage embryos obtained by *in vitro* fertilization until the blastocyst stage and established ES cell lines as described previously (4, 31). The cell lines obtained were genotyped as described above. For tetraploid aggregation experiments, two-cell-stage embryos derived from crosses of BDF1 females with ICA;CAG-EGFP-IRES-puromycin males (in which the EGFP gene was ubiquitously expressed) were collected in KSOM medium (ARK Resource, Kumamoto, Japan). Embryos were then equilibrated in fusion buffer (0.3 M mannitol, 0.1 mM $MgSO_4$, polyvinyl alcohol [0.1 mg/ml], bovine serum albumin F-V [3 mg/ml; Sigma]) and placed between the electrodes of an electrofusion chamber (1-mm gap). Electrofusion was performed using a pulse generator (ECM2001; BTX, San Diego, CA) by application of two 40-μs pulses at 80 V/cm. Fused embryos were cultured in KSOM medium at 37°C for 40 h. $Cdh1^{GT/GT}$ or wild-type ES cells were then aggregated with the tetraploid embryos and transferred to pseudopregnant foster mothers (29, 31).

Scanning electron microscopy. The eyelids of embryos at 14.5 to 18.5 dpc were dissected under a stereoscopic microscope and fixed in 0.1 M sodium phosphate buffer (pH 7.4) containing 2% glutaraldehyde and 2% formaldehyde. Samples were washed and dehydrated in a graded series of ethanol, dried, sputter coated according to standard procedures, and then examined under a scanning electron microscope.

RESULTS

Effects of Cdh1 ablation on actin cytoskeleton organization. The role of Cdh1 has been investigated mainly as a regulator of the cell cycle using mammalian cultured cells or model organisms, such as flies and *Saccharomyces cerevisiae* (35). To further elucidate the physiological functions of Cdh1, we analyzed *Cdh1* gene-trapped (GT) mice generated using the exchangeable pU-17 GT vector, which encodes the β-galactosidase-neomycin resistance (β-*geo*) fusion gene (see Fig. S1 in the supplemental material). Homozygous *Cdh1* GT ($Cdh1^{GT/GT}$) mouse embryonic fibroblasts (MEFs) had a severely reduced abundance of Cdh1 expression, both at the RNA (less than 2% of that observed in wild-type MEFs) and protein levels (see Fig. S1). To investigate the role of Cdh1 on mammalian cellular behavior, we first analyzed asynchronously proliferating $Cdh1^{GT/GT}$ MEFs using time-lapse microscopy. We noticed a slight reduction in the cellular motility of $Cdh1^{GT/GT}$ MEFs compared with wild-type MEFs (data not shown). One possible reason for this difference could be proliferation defects in $Cdh1^{GT/GT}$ MEFs. To explore other possibilities, we focused on actin cytoskeletal architecture, which also plays an important role in cell motility. We compared the distribution of F-actin between $Cdh1^{GT/GT}$ MEFs and control cells (Fig. 1A). Immunofluorescence analysis of Alexa Fluor 488-conjugated phalloidin-labeled cells revealed that Cdh1 deficiency led to a striking phenotype that was characterized by fewer bundled actin stress fibers in the cell body and a more disorganized appearance (Fig. 1A, frames a and b). We quantified stress fiber density by incorporating a line profile across the cytoplasm that identified stress fibers by their increased fluorescence relative to areas devoid of stress fibers (Fig. 1B). Sharp, distinct peaks in fluorescence intensity within each line profile represented individual stress fibers crossed by the lines, as shown in Fig. 1B. Quantification of these peaks showed a significant decrease in $Cdh1^{GT/GT}$ MEFs compared with wild-type cells; however, the formation of cortical actin was preserved in $Cdh1^{GT/GT}$ MEFs (Fig. 1B). To further confirm the observation from MEFs, we transfected HeLa cells with an siRNA oligonucleotide against Cdh1 (Fig. 1C) and then analyzed the cytoskeletal architecture of these cells. *Cdh1*-deficient cells showed reduced stress fiber organization (Fig. 1C, frames a and b). The inhibitory effect of Cdh1 on actin stress fiber formation was enhanced under serum-free culture conditions (Fig. 1C, frames c and d). Moreover, we used the N-terminal fragment of Cdh1 (DN-Cdh1), which lacks the substrate-binding C terminus of Cdh1 and functions in a dominant negative fashion (54), to evaluate the role of Cdh1 in stress fiber formation. HeLa cells that expressed GFP–DN-Cdh1 tended to display a flattened shape, had reduced stress fibers, and exhibited reorganized cortical actin compared with surrounding nontransfected cells (Fig. 1D and E). The expression of DN-Cdh1 had the same effect on stress fibers in NIH 3T3 cells as in HeLa cells (Fig. 1F). These results suggest that Cdh1 played a regulatory role in the actin cytoskeleton of cells of different origins.

Focal adhesion remodeling usually accompanies actin rearrangements (42). We next examined whether actin fiber disassembly in *Cdh1*-deficient cells correlated with changes in FA formation. Immunostaining of paxillin, which is a major component of FAs, revealed that paxillin-labeled FAs were reduced in size and number, both in $Cdh1^{GT/GT}$ MEFs and in *Cdh1*-depleted HeLa cells (Fig. 1A, frames c and d, and C, frames e and f). We also observed that serum starvation reduced paxillin expression substantially in *Cdh1*-depleted cells (Fig. 1C, frames g and h). Collectively, our data suggest that Cdh1 played a role in the formation of FAs and stress fibers.

Cdh1 regulated Rho GTPase activity. Rho GTPases are important regulators of the actin cytoskeleton. To address the molecular mechanisms of stress fiber disassembly in

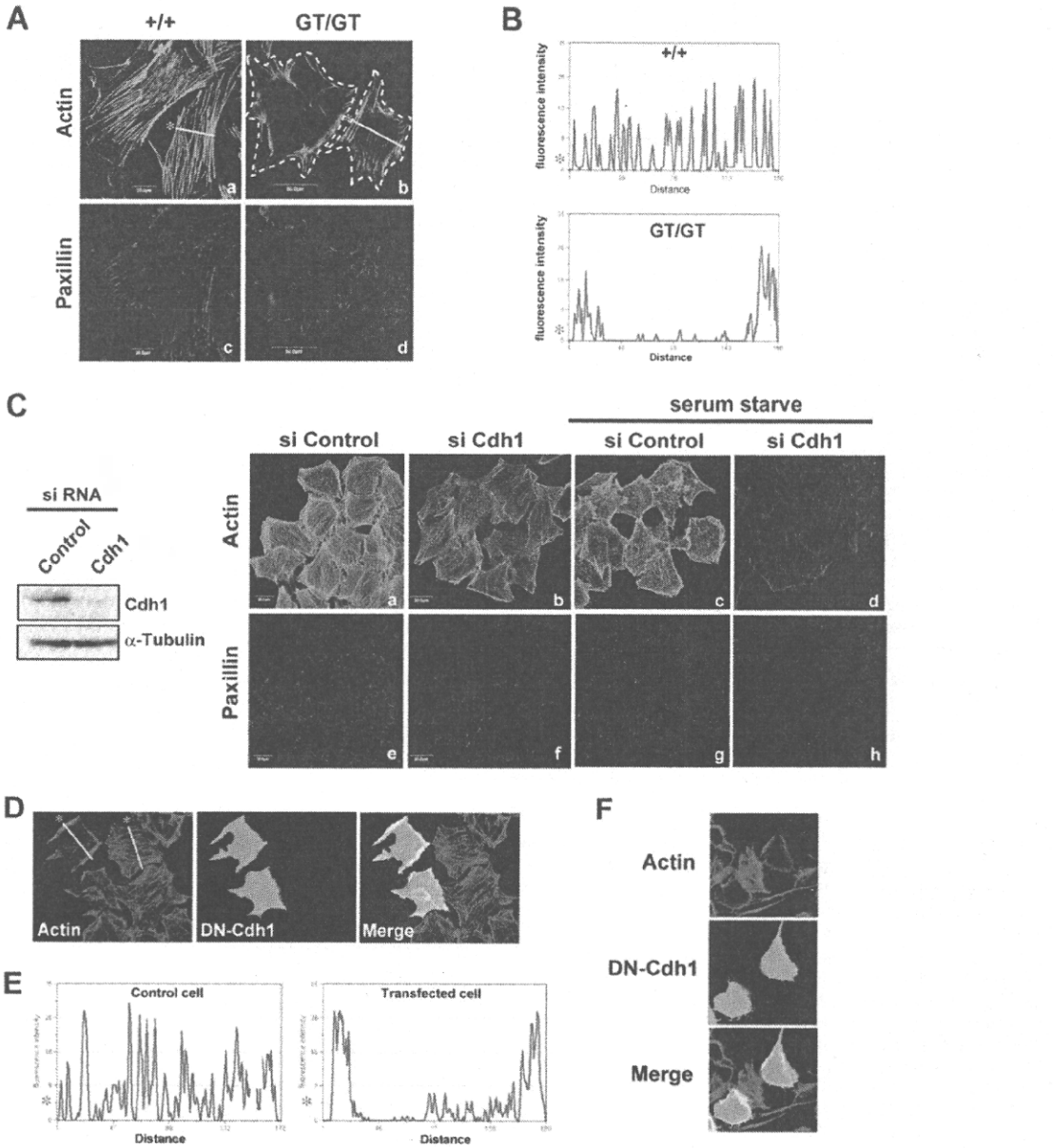

FIG. 1. Effects of Cdh1 depletion on the actin cytoskeleton in mouse embryonic fibroblasts (MEFs) and HeLa cells. (A) Primary MEFs derived from *Cdh1*$^{+/GT}$ mouse intercrosses were fixed and stained with Alexa Fluor 488-conjugated phalloidin (green) and with an antipaxillin antibody (red). The areas outlined by the dotted lines depict the cell bodies of *Cdh1*$^{GT/GT}$ MEFs. Bars, 20 μm (a and c) and 50 μm (b and d). (B) Quantification of fluorescent intensity across the yellow lines shown in the corresponding panels in A (to indicate stress fiber density) using the MetaXpress software (Molecular Devices). The asterisks denote the cells quantified in panel A and their corresponding line graphs B. (C) HeLa cells were transfected with a control siRNA oligonucleotide or with an siRNA oligonucleotide against Cdh1 and cultured for 2 days. The levels of expression of Cdh1 were evaluated using immunoblot analysis (left panels). HeLa cells transfected as described above were cultured in medium containing 10% serum (frames a, b, e, and f) or in serum-free medium (frames c, d, g, and h) for 24 h, fixed, and stained with Alexa Fluor 488-phalloidin (upper panels) and with an antipaxillin antibody (lower panels). Bars, 20 μm. (D) HeLa cells were transfected for 24 h with a GFP-tagged N-terminal fragment (residues 1 to 125) of Cdh1, which lacks the substrate-binding domain (WD-40 repeats) and acts in a dominant negative (DN) fashion (DN-Cdh1). Cells were then stained for rhodamine-phalloidin. (E) Quantification of fluorescence intensity across the yellow lines shown in panel D, as described for panel B. (F) NIH 3T3 cells were treated and analyzed as in panel D.

Cdh1$^{GT/GT}$ MEFs, we examined the abundance of Rho-family GTPases in these cells. We observed no significant differences in the protein expression levels of the Rho GTPases analyzed, with the exception of cdc42, which was not detected in MEFs (Fig. 2A). Thereafter, we focused on Rho because of its central role in the regulation of contractile actin-myosin stress fibers and of the assembly of FAs (38). RhoGDI has been shown to regulate Rho activity by binding GDP-bound RhoA (33). However, we found no changes in the levels of RhoGDI in *Cdh1*$^{GT/GT}$ MEFs (Fig. 2A), which excludes the possibility that

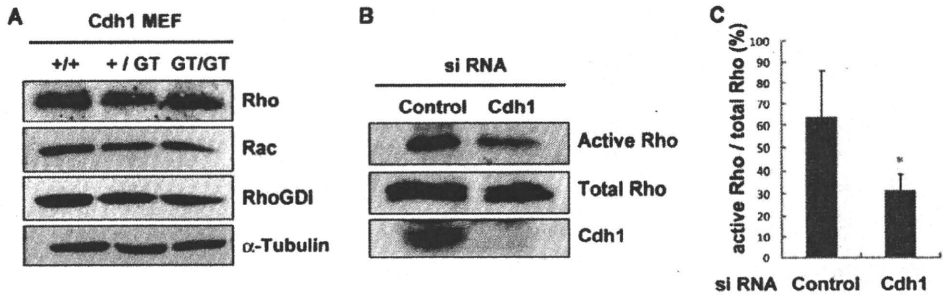

FIG. 2. Rho activity was decreased in *Cdh1*-depleted cells. (A) Cell lysates from wild-type or $Cdh1^{GT/GT}$ MEFs adjusted to equal protein concentrations were electrophoresed and transferred to nitrocellulose for immunoblot analysis using anti-Rho, anti-Rac, and anti-RhoGDI antibodies. α-Tubulin levels are shown as a loading control. (B) 293T cells were transfected with an siRNA directed against Cdh1 or with a control and were lysed after 2 days of cell culture. The GST-rhotekin RBD was incubated with the cell lysates to pull down active Rho. The levels of RBD-bound Rho and total Rho in cell lysates were determined by immunoblotting using an anti-Rho antibody. A representative result of three individual experiments is shown. (C) Quantification of the immunoblotting data in panel B was performed using densitometry. Data (arbitrary units) were normalized to the amount of total Rho and represent means ± standard deviations from three independent experiments (*, $P < 0.05$, Student's *t* test).

Cdh1 regulated Rho activity via the upregulation of its GDP-bound inactive form. We next analyzed Rho activity by affinity precipitation assay using a GST fusion protein containing the RhoA-binding domain of rhotekin (36, 37). 293T cells were stimulated with LPA for 10 min before harvesting, and the levels of bound active RhoA were measured. As shown in Fig. 2B, Cdh1 siRNA-transfected cells showed a marked decrease in GTP-bound Rho protein compared with control cells. Quantification of Rho activity revealed that Cdh1 depletion reduced Rho activity substantially, i.e., to 49% of the activity measured in control cells (Fig. 2C). Together with the data shown in Fig. 1, these results demonstrated the previously unknown role of Cdh1 as a regulator of Rho GTPase.

Cdh1 depletion led to p190 RhoGAP accumulation. p190 RhoGAP (p190) is ubiquitously expressed in various tissues and functions exclusively toward Rho *in vivo*. Furthermore, p190 activity accounts for ~60% of the total RhoGAP activity when activity is assessed in fibroblast cell extracts (52). We observed a significant reduction of actin stress fiber formation in $Cdh1^{GT/GT}$ MEFs, which is consistent with a phenotype of Rho inhibition (Fig. 1A). Hence, we assumed that APC/C^{Cdh1} may target p190 directly as a substrate for degradation. To test this possibility, we compared the expression levels of p190 in $Cdh1^{GT/GT}$ MEFs with those of wild-type cells using immunoblot analysis. Consistent with the results reported for the known APC/C^{Cdh1} substrate Skp2 (6, 56), p190 accumulated substantially in $Cdh1^{GT/GT}$ MEFs (1.94-fold compared with wild-type MEFs) (Fig. 3A). We used quantitative real-time PCR analysis to confirm that the observed difference in p190 abundance was not due to transcriptional upregulation (Fig. 3B). To further examine whether Cdh1 had a negative impact on the expression of the p190 protein, we interfered with Cdh1 function in HeLa cells via transfection of an siRNA oligonucleotide against Cdh1 or of a dominant negative mutant Cdh1 expression vector (54) and analyzed their effect on p190 abundance. Impairment of Cdh1 function led to the accumulation of the p190 protein (Fig. 3C and D). Simple overexpression of wild-type Cdh1 had no effect on the expression levels of p190 or on cellular morphology (Fig. 3D and data not shown), which implies that exogenously induced Cdh1 did not activate APC/C efficiently. To address this issue, we depleted early mitosis inhibitor 1 (Emi1), which is an inhibitor of APC/C^{Cdh1}, to catalytically activate endogenous APC/C^{Cdh1} in interphase HeLa cells (12, 27). We analyzed HeLa cells transfected with siRNA oligonucleotides against Emi1 and found that p190 expression levels were reduced significantly in these cells (Fig. 3E, first panel). Another known target of APC/C^{Cdh1}, cyclin B1, was also decreased after Emi1 depletion (Fig. 3E, arrow in the second panel). Furthermore, the decreased p190 levels in Emi1-depleted HeLa cells were restored by proteasome inhibitor treatment (Fig. 3E). These results support the notion that APC/C^{Cdh1} regulated p190 abundance via the ubiquitin-proteasome system.

A previous study indicated that the levels of p190 oscillate in a cell cycle-dependent manner; they are elevated from interphase to mid-mitosis and decline after entry into late mitosis (45). Therefore, loss of Cdh1 function during the cell cycle, especially on mitotic exit, may affect the abundance of p190. To rule out this possibility, we analyzed the cell cycle profiles of $Cdh1^{GT/GT}$ MEFs and Cdh1-depleted HeLa cells using flow cytometry. Consistent with a previous report (15), the Cdh1-depleted cell population contained a slightly elevated number of cells that were in the G_2/M phase of the cell cycle (Fig. 3F), which suggests slower mitotic progression. As a shortened mitosis can cause secondary p190 accumulation, these results indicate that cell cycle alteration in Cdh1-depleted cells may be unfavorable to p190 protein accumulation. Therefore, the role of Cdh1 during the cell cycle seems to be independent from the regulation of p190 abundance.

APC/C^{Cdh1}-mediated ubiquitination of p190. Cdh1 recognizes and binds target motifs on its substrate (35). The destruction (D) and KEN boxes are most prominent among the targeting motifs of APC/C substrates for degradation. p190 has five D boxes and two KEN boxes in its full sequence (Fig. 4A). To determine whether p190 was a direct target of APC/C^{Cdh1}, we performed an *in vitro* binding assay using several p190 mutants. As shown in Fig. 4B, both full-length p190 and the middle domain (MD) of p190 were coprecipitated with *in vitro* translated Cdh1 (Fig. 4B). Furthermore, deletion mutants containing only KEN-box (MD-N) and D-boxes (MD-C) were also

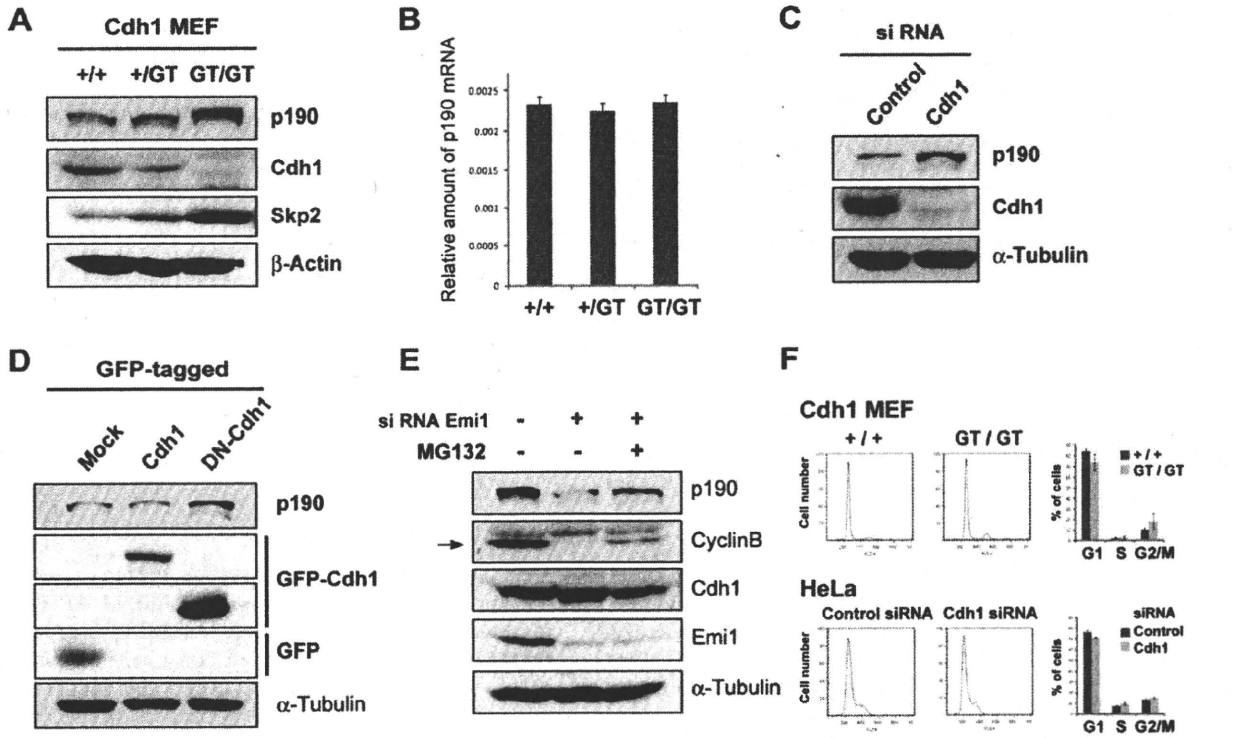

FIG. 3. p190 was stabilized in *Cdh1*-deficient cells. (A) Primary MEFs of the indicated genotypes were collected, lysed, and immunoblotted for endogenous p190, Cdh1, and Skp2. β-Actin levels are shown as a loading control. Each experiment was conducted in triplicate, and the immunoblots presented here are representative runs. (B) An abundance of p190 proteins was regulated posttranslationally. Total RNA was isolated from MEFs of the indicated genotypes and subjected to quantitative RT-PCR analysis of the p190 mRNA. Data were normalized to the levels of GAPDH mRNA and represent means ± standard deviations from three independent experiments. (C) Accumulation of p190 in *Cdh1*-depleted HeLa cells. HeLa cells were transfected with either control or Cdh1 siRNA oligonucleotides. After 48 h of culture, cells were harvested and examined for the expression levels of p190, Cdh1, and α-tubulin using immunoblotting analysis. (D) HeLa cells were transfected with GFP-tagged full-length Cdh1 or DN-Cdh1 expression vectors. Cells were lysed and processed through immunoblotting using antibodies against p190, GFP, and α-tubulin. (E) Cdh1 activation caused a reduction in the levels of p190. HeLa cells transfected with control or Emi1 siRNA oligonucleotides were cultured for 48 h in the absence (−) or presence (+) of MG132. Cell lysates were subjected to SDS-PAGE and immunoblot analysis using the indicated antibodies. Emi1 depletion led to Cdh1 activation, as evidenced by the degradation of its target, cyclin B (arrow, middle lane). (F) Flow cytometric analysis of the cell cycle. Asynchronous MEFs with the indicated genotypes and HeLa cells that were transfected with either control or Cdh1 siRNA oligonucleotides for 24 h were stained with propidium iodide and were then subjected to flow cytometry. The percentage of cells in each phase of the cell cycle is shown.

bound to Cdh1 (Fig. 4B), which indicates the relevance of each box for the interaction with Cdh1. We next examined the *in vivo* interaction between Cdh1 and p190. Immunoprecipitation of the lysate that expressed GFP-fused full-length Cdh1 using the p190 antibody led to the identification of exogenous Cdh1 in the complex (Fig. 4C). To confirm the physiological interaction between these proteins, we prepared a Cdh1-specific antibody by immunizing rabbits with mouse Cdh1 N-terminal peptides. Using this polyclonal antibody, we found that endogenous p190 coprecipitated with endogenous Cdh1 (Fig. 4D).

We next examined whether the abundance of p190 was regulated via the ubiquitin–proteasome system. Coexpression of GFP-p190 with HA-tagged ubiquitin in 293T cells revealed that p190 was ubiquitinated predominantly in the presence of the proteasome inhibitor (Fig. 5A), which supports the notion that p190 is ubiquitinated *in vivo* (45). However, 293T cells transfected with an siRNA oligonucleotide against Cdh1 exhibited a substantial reduction in the ubiquitination of endogenous p190 (Fig. 5B) to ~60% of that observed in control cells (Fig. 5C). Furthermore, the decrease in the ubiquitination of p190 in immortalized $Cdh1^{GT/GT}$ MEFs was restored by the addition of wild-type Cdh1 in a dose-dependent manner (Fig. 5D). We next examined whether the APC/C^{Cdh1} complex ubiquitinated p190 directly using an *in vitro* ubiquitination assay. We incubated immunopurified HeLa APC/C with or without recombinant His-tagged full-length Cdh1 protein purified from Sf9 cells. The resultant APC/C^{Cdh1} complex was analyzed for its ability to support the ubiquitination of *in vitro* translated p190 in a reconstituted reaction mixture containing purified E1 and E2 enzymes (22). As shown in Fig. 5E, APC/C ubiquitinated p190 effectively *in vitro* when Cdh1 was present in the reaction mixture.

Cdh1 regulated cellular motility via control of p190 abundance. As the coordinated regulation of Rho activity is important for cell migration (13), we investigated whether Cdh1 deficiency affected cellular movement. The migration ability of Cdh1 knockdown HeLa cells was examined using a Boyden chamber migration assay. Serum-deprived siRNA-transfected HeLa cells were plated onto the membrane of a Boyden chamber in the absence of any stimuli and were allowed to migrate

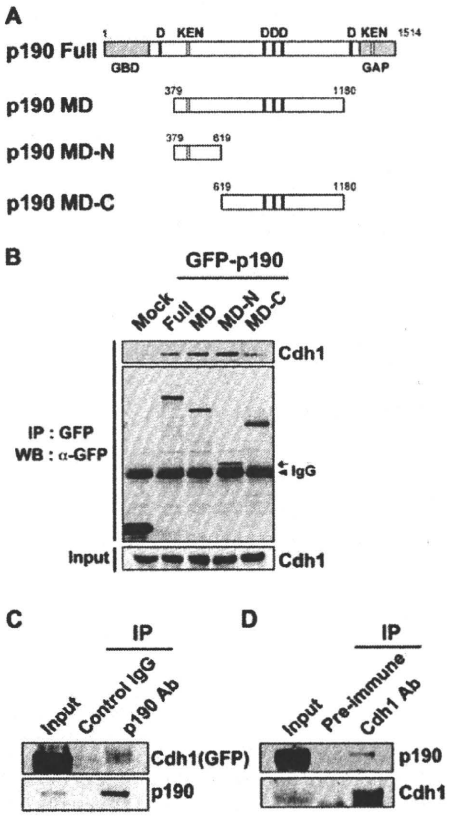

FIG. 4. The middle domain of p190 interacted with Cdh1. (A) Schematic representations of the structure of p190 and its derived mutants. MD, middle domain; GBD, GTP-binding domain; GAP, GTPase-activating domain. (B) *In vitro* binding assay. The indicated GFP-p190 proteins expressed in 293T cells were immunopurified, immobilized on protein A beads (Dynal), and incubated with *in vitro* translated Cdh1. The resulting immunocomplex was analyzed using avidin-HRP to detect the bound biotin-Cdh1. The arrow indicates the MD-N mutant for p190. The arrowhead indicates IgG. (C) Lysates from 293T cells transfected with GFP-tagged full-length Cdh1 were immunoprecipitated using control rabbit IgG or an antibody (Ab) against p190. These immunoprecipitates were then fractionated by SDS-PAGE and immunoblotted using an anti-GFP antibody (top) or an anti-p190 antibody (bottom). (D) *In vivo* coimmunoprecipitation of p190 with Cdh1. Lysates from 293T cells were immunoprecipitated with rabbit preimmune serum or serum against Cdh1. These immunoprecipitates were then fractionated by SDS-PAGE and immunoblotted using anti-p190 (top) or anti-Cdh1 (bottom) antibodies. IP: immunoprecipitation; WB, Western blotting.

for 24 h. Unstimulated HeLa cells exhibited virtually no motility (Fig. 6C, first bar). Stimulation of HeLa cells with FBS led to an increase in their migratory activity compared with unstimulated HeLa cells (Fig. 6A, left panel, and C, second bar). Importantly, Cdh1 knockdown cells exhibited very low motility, even when stimulated by FBS (Fig. 6A, middle panel, and C, third bar). To determine if Cdh1 and its substrate p190 acted in a linear pathway to regulate cellular motility, we performed an epistatic analysis of the effects of Cdh1 and p190 knockdown on a cell migration assay. We optimized co-knockdown conditions to deplete p190 in *Cdh1*-knockdown cells to levels comparable to those of control cells (Fig. 6B). The combination of both Cdh1 and p190 RNAi rescued the motility defect of Cdh1 knockdown HeLa cells significantly to ~110% of the level observed in control cells (Fig. 6A, right panel, and C, fourth bar).

Given that p190-mediated regulation of Rho is important for cell migration, how does Cdh1 affect p190 activity? It is known that the activity of p190 is regulated by phosphorylation (5, 30). We speculated that the level of expression of p190 may also be a key factor to control its RhoGAP activity. To examine this hypothesis, we analyzed the distribution of F-actin in p190 knockdown cells at different time points. As shown in Fig. 6D and E, the extent of stress fiber formation of p190 knockdown HeLa cells was inversely correlated with the abundance of p190. Furthermore, when p190 was exogenously overexpressed in MEFs or NIH 3T3 cells, these cells had reduced stress fibers and exhibited reorganized cortical actin compared with surrounding nontransfected cells (Fig. 6F, upper row, and G) as in dominant negative Cdh1-expressing cells (Fig. 1D and F). These results suggest that p190 abundance plays a key role in its RhoGAP activity. We also confirmed that the actin phenotype of $Cdh1^{GT/GT}$ MEFs was rescued by introducing wild-type Cdh1 (Fig. 6F, lower row). These findings are consistent with the notion that APC/C^{Cdh1} and p190 operate in a linear pathway, where p190 acts downstream of APC/C^{Cdh1} in the control of Rho GTPase.

Physiological role of Cdh1 during murine development. To analyze the relevance of Cdh1-mediated regulation of Rho *in vivo*, we analyzed $Cdh1^{GT/GT}$ mice. Among the 152 mice that were the progeny of the intercross of $Cdh1^{+/GT}$ mice, no $Cdh1^{GT/GT}$ animals were detected at weaning (see Table S1 in the supplemental material), which confirmed that homozygous loss of *Cdh1* resulted in embryonic death (15, 24). To determine the timing and nature of this mortality, we examined the morphology and viability of embryos from timed $Cdh1^{+/GT}$ intercrosses. Viable embryos were defined by the detection of a heartbeat at 11.5 to 13.5 dpc. The number of viable $Cdh1^{GT/GT}$ embryos decreased with developmental progression, with none remaining alive at 13.5 dpc (see Table S1). These results thus suggest that embryonic death was initiated at around 10.5 to 12.5 dpc. We also confirmed that the death of $Cdh1^{GT/GT}$ embryos was attributable to the *Cdh1* GT using a KI rescue experiment (see Fig. S2 in the supplemental material).

The mouse placenta consists of three layers, which, starting from the embryonic side, are known as the labyrinth, the spongiotrophoblast, and the trophoblast giant cell (TGC) layers (Fig. 7A, top panel) (34). In contrast with the thin layer of TGCs present beneath the maternal decidua in wild-type placentas, cells with giant nuclei were not detected in $Cdh1^{GT/GT}$ placentas, as assessed by either hematoxylin-eosin or Feulgen staining (see Fig. S3 in the supplemental material). This implies that the endoreplication of TGC was compromised in $Cdh1^{GT/GT}$ placentas (15, 24). Cdh1 was expressed in the labyrinth layer of $Cdh1^{+/GT}$ placentas, as revealed by whole-mount X-Gal staining (see Fig. S3). Hematoxylin-eosin staining of $Cdh1^{GT/GT}$ placentas at 12.5 or 13.5 dpc revealed the presence of frequent abnormal thrombi in the labyrinth layers (Fig. 7A, middle panel, and B). Furthermore, the labyrinth layer of $Cdh1^{GT/GT}$ placentas exhibited an abnormal vasculature compared with that of their wild-type counterparts (Fig.

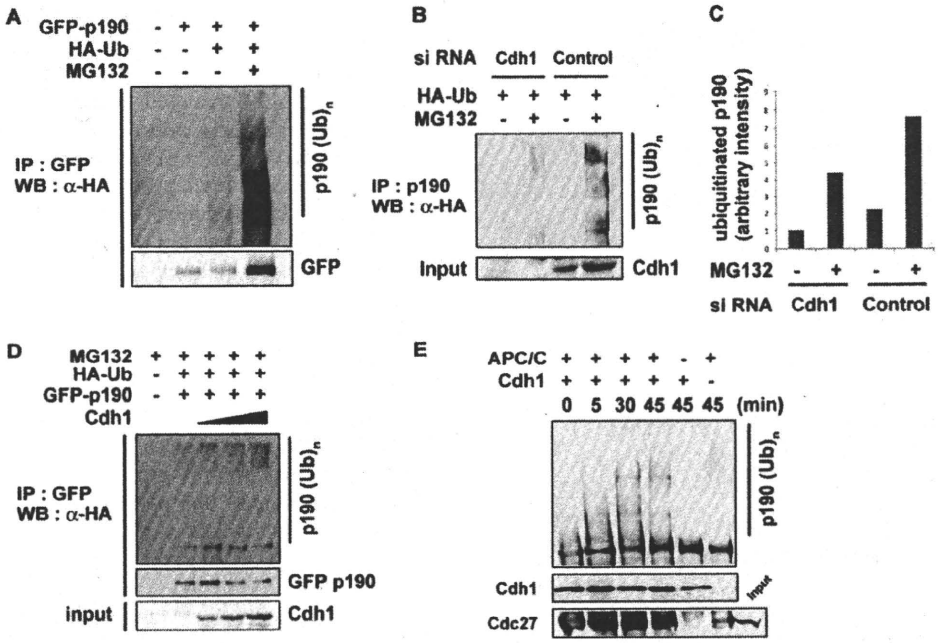

FIG. 5. APC/C^{Cdh1}-mediated ubiquitination of p190. (A) *In vivo* ubiquitination of p190. 293T cells were transfected with the GFP–full-length p190 expression plasmid or control vector, together with an HA-ubiquitin expression plasmid in the presence or absence of MG132. Lysates were immunoprecipitated (IP) with an anti-GFP antibody and were immunoblotted (Western blotting [WB]) using anti-HA (α-HA) and anti-GFP antibodies. (B) 293T cells transfected with either control or Cdh1 siRNA oligonucleotides for 48 h were subjected to an *in vivo* ubiquitination assay, as described for panel A. (C) Quantification of the ubiquitinated p190 protein in panel B was performed using densitometry. The value obtained for Cdh1 siRNA-transfected cells without MG132 treatment was set as 1. (D) Immortalized $Cdh1^{GT/GT}$ MEFs were transfected with GFP-full-length p190, HA-ubiquitin (Ub), and full-length Cdh1 expression vectors. *In vivo* ubiquitination of p190 was evaluated as described for panels A and B. (E) *In vitro* ubiquitination assay. APC/C immunoprecipitated from HeLa cell lysates was conjugated with recombinant Cdh1 protein and was then subjected to an *in vitro* ubiquitination assay, as described in Materials and Methods. *In vitro* translated full-length p190 was used as a substrate. The reaction was terminated at the indicated time points. Ubiquitinated p190 was detected by immunoblotting with anti-p190 antibody (top panel). Recombinant His-Cdh1 protein used for APC/C binding was immunoblotted using anti-His antibody (middle). The presence of APC/C complex in each reaction product was confirmed by Western blotting against cdc27 (bottom). The input lane represents 0.5% of HeLa cell lysate used for immunoprecipitation.

7A). These phenotypes were similar to *ROCK II* (also known as Rho-kinase or ROK α) knockout (KO) mice (49).

To examine whether placental insufficiency was a central cause of embryonic lethality, we performed tetraploid complementation rescue experiments (Fig. 7A, bottom panel; see also Fig. S4 in the supplemental material). We found that $Cdh1^{GT/GT}$ embryos survived beyond the organogenesis stage to 18.5 dpc in this system. The placental deficiencies of $Cdh1^{GT/GT}$ mice somewhat resembled those of *ROCK II* KO mice; however, in contrast to what was observed in *ROCK II* KO mice, blood clots in peripheral limbs were not observed in $Cdh1^{GT/GT}$ animals. Eyes open at birth and omphalocele are significant phenotypes of *ROCK I* (also known as ROK β) KO mice (44). During normal mouse development, eyelid closure occurs between 15.5 and 16.5 dpc via extension of the ridges of the epithelium at its periphery (14). To explore whether Cdh1 deficiency caused a defect in this developmental process, we analyzed $Cdh1^{GT/GT}$ embryos rescued using tetraploid complementation experiments. We used wild-type ES cell lines that were established concomitantly with $Cdh1^{GT/GT}$ ES cell lines (see Materials and Methods) as a control for tetraploid aggregation. Tetraploid complementation itself affects the timing of eyelid closure, as all wild-type embryos examined ($n = 4$) had open eyelids at 15.5 dpc; however, this was reduced to 22.2% of embryos ($n = 9$) at 18.5 dpc (Fig. 7C to F). In contrast, 83.3% of $Cdh1^{GT/GT}$ embryos exhibited an open-eye phenotype ($n = 10$) at 18.5 dpc, which suggests a significant role for Cdh1 in eyelid closure (Fig. 7C to F). Conversely, we did not observe increased omphalocele in $Cdh1^{GT/GT}$ embryos (data not shown). Eyelid closure is regulated by complicated mechanisms, as other signaling pathways, such as the mitogen-activated protein (MAP) kinase cascade, are also involved in this process (44). To explore whether Cdh1 regulated eyelid closure via the Rho/ROCK pathway, we analyzed the abundance of p190 in the eyelid epithelial sheet. Immunohistochemical analysis of p190 showed that staining for p190 was more pronounced in the eyelid epithelial sheet of $Cdh1^{GT/GT}$ embryos than in wild-type embryos (Fig. 7G). Furthermore, p190 accumulated in the brain and spinal cord of $Cdh1^{GT/GT}$ embryos, where p190 mRNA is expressed specifically at high levels (10) (Fig. 7H). These results strongly suggest that Cdh1 is an important regulator of the *in vivo* Rho/ROCK signaling via p190.

DISCUSSION

In the present study, we identified a novel function for the APC/C activator Cdh1 on the regulation of Rho subfamily GTPases. Rho promotes the formation of actin stress fibers

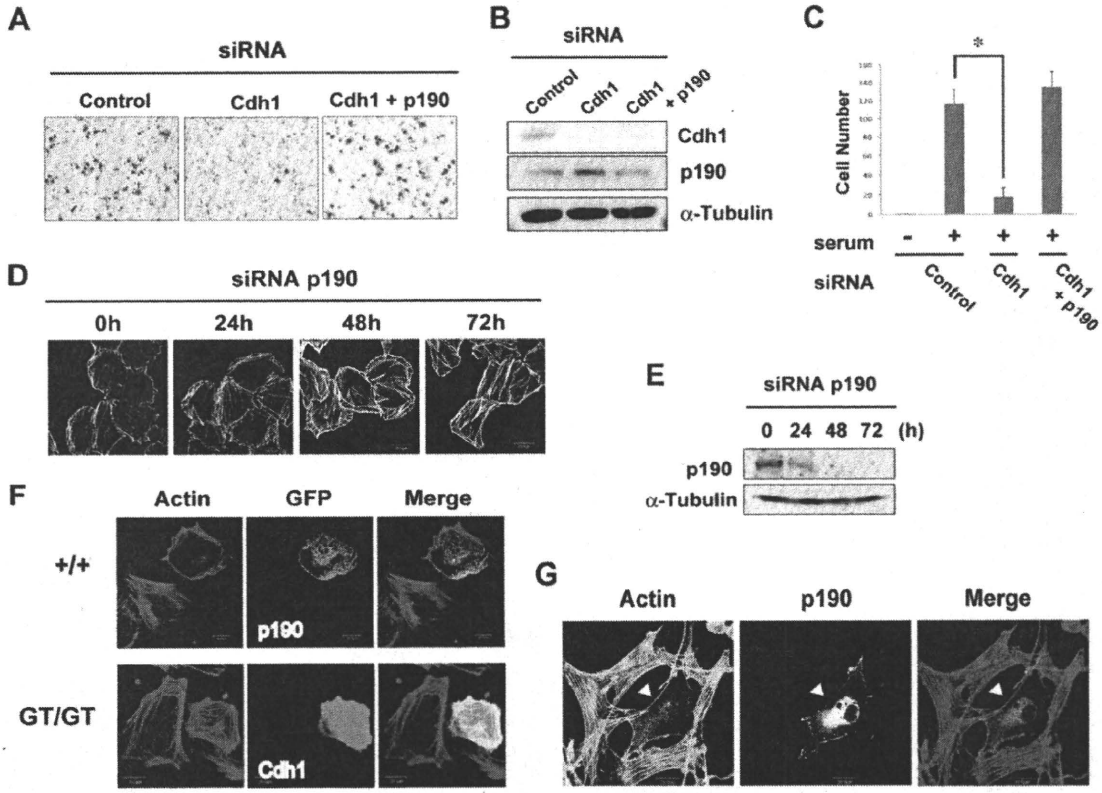

FIG. 6. Cdh1 regulated cell motility via control of p190 abundance. (A) siRNA-transfected HeLa cells were placed on membranes in serum-free medium after 48 h of culture and were allowed to migrate in a Boyden chamber for 24 h, either in the absence of any stimuli or in the presence of 10% FBS. Membranes were then fixed and stained with 50% Giemsa solution in PBS. Data shown were representative of migrating cells transfected with the indicated siRNA oligonucleotides. (B) The levels of Cdh1 and p190 in cells subjected to a Boyden chamber assay were assessed by immunoblot analysis using anti-Cdh1 and anti-p190 antibodies. The corresponding α-tubulin levels are shown as a loading control. (C) Migration was assessed as the number of cells that invaded the membrane after 24 h of incubation. Data represented mean values ± standard errors of the means from measurements performed in triplicate from three independent experiments using HeLa cells (*, $P < 0.05$, Student's two-tailed t test). (D) HeLa cells were transfected with siRNA oligonucleotides against p190 and cultured for 0 to 48 h in the medium containing 10% FBS. After 48 h, the cell medium was replaced with serum-free DMEM-F12. Cells were fixed and stained with Alexa Fluor 488-phalloidin at the indicated times. (E) HeLa cells were transfected and cultured as described for panel D. Cells were harvested and examined for the expression levels of p190 and α-tubulin using immunoblot analysis. (F) Primary wild-type (upper row) and *Cdh1*$^{GT/GT}$ (lower row) MEFs were transfected for 24 h with GFP-p190 and GFP–wild-type Cdh1, respectively. Cells were fixed and stained with rhodamine-phalloidin. (G) NIH 3T3 cells were transfected for 24 h with GFP-p190. Cells were fixed and stained with Alexa Fluor 488-phalloidin. The arrowhead indicates p190 transfected cells. Bars, 100 μm (A) and 20 μm (D, F, and G).

and FAs by activating its downstream effectors, i.e., ROCK and mDia (mammalian homolog of the *Drosophila* gene *Diaphanous*) (32). ROCK induces stress fiber formation via the phosphorylation of myosin phosphatase and LIM kinase in nonmuscle cells (2). It has been reported that ROCK inhibition blocks myosin light chain phosphorylation and the subsequent formation of stress fibers in the center, but not at the periphery, of cells (50). Cdh1-depleted cells significantly reduced the formation of actin filament bundles at the cell body; however, it was retained at cell periphery (Fig. 1B and E), which implies the presence of ROCK suppression in these cells. mDia also regulates actin filament formation and adhesion turnover via the mobilization of adenomatous polyposis coli and c-Src (58). FAs are specialized adhesive structures in which integrin, a receptor of the extracellular matrix, and numerous signaling components are concentrated (11). The importance of the actin cytoskeleton in FA assembly has been demonstrated in experiments where inhibition of the actin-myosin interaction promotes disassembly of FAs (42). Consistently, we found that the Cdh1 deficiency caused a reduction of both stress fiber and FA assembly, with a decreased level of active Rho (Fig. 1 and 2). This Rho-mediated response acts downstream of the signaling activated by growth factors (38, 42). Serum starvation of cells transfected with Cdh1 siRNA resulted in further attenuation of the assembly of stress fibers and FAs compared with cells with Cdh1 knockdown only (Fig. 1C), which indicates that multiple signals, including the Cdh1/p190 axis, seem to converge during Rho regulation. Rho-mediated actin cytoskeleton formation is controlled at multiple levels. Elevation of cyclic AMP (cAMP) levels and the consequent activation of protein kinase A (PKA) lead to loss of stress fibers and FAs via the phosphorylation of the myosin light chain kinase and Rho (42). It was reported that PKA also phosphorylates APC/C and inhibits its ubiquitination activity, even in the presence of Cdh1 (21). Therefore, we could speculate that cAMP/PKA regulates the actin cytoskeleton also via an APC/C^{Cdh1}/p190/Rho pathway.

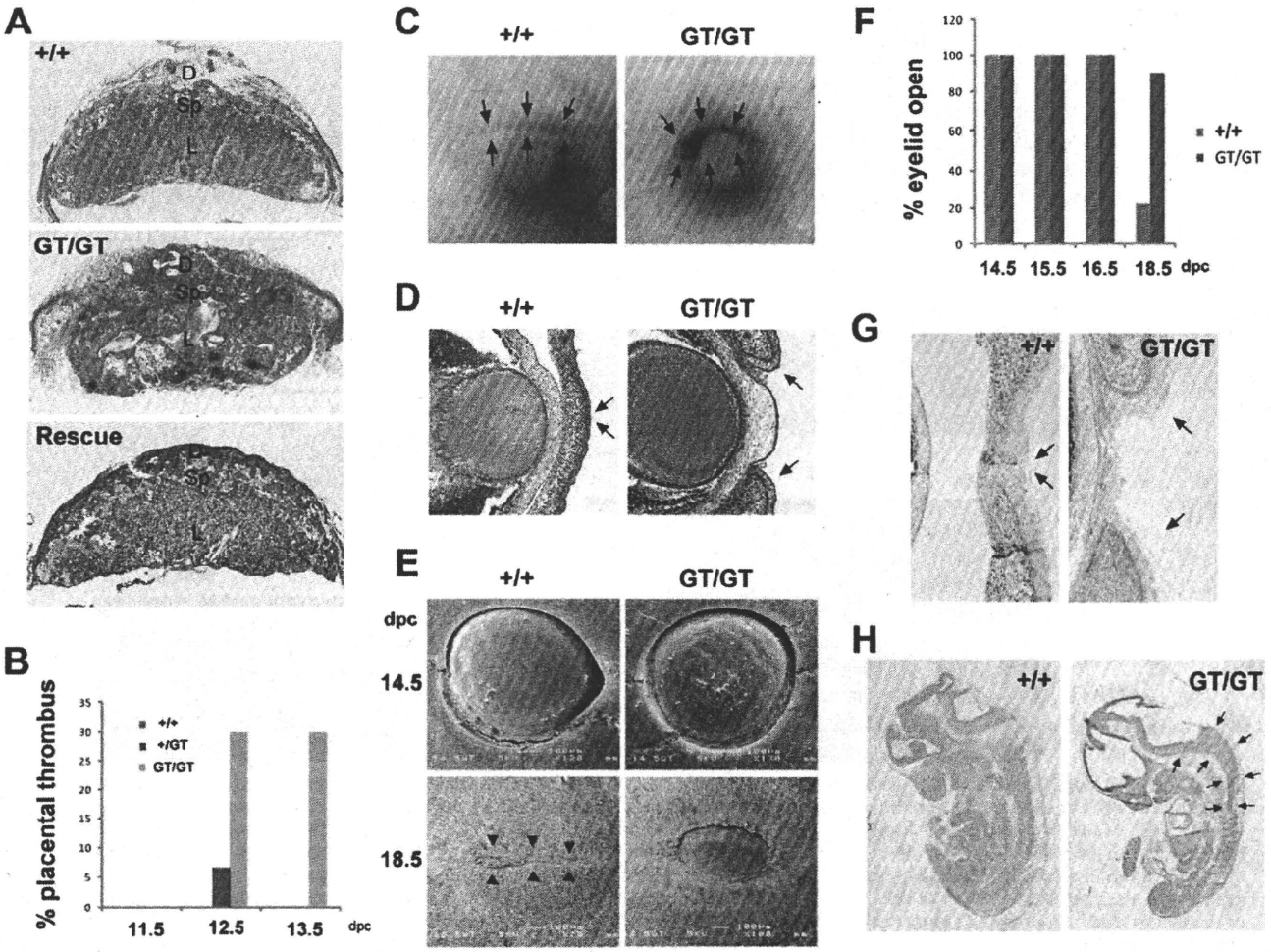

FIG. 7. Developmental defects of *Cdh1*$^{GT/GT}$ embryos. (A) Hematoxylin-eosin staining of sections of wild-type, *Cdh1*$^{GT/GT}$, or tetraploid complementation-rescued placentas at 12.5 dpc. The asterisk indicates thrombus in the labyrinth layer. D, decidua; Sp, spongiotrophoblast layer; L, labyrinth layer. (B) Percentage of placentas with thrombus formation at the indicated dpc. Placentas with thrombus that had a diameter larger than 500 μm (longest diameter) were judged as positive. The number of placentas analyzed was as follows: at 11.5 dpc, *Cdh1*$^{+/+}$, 5; *Cdh1*$^{GT/+}$, 8; and *Cdh1*$^{GT/GT}$, 7; at 12.5 dpc, *Cdh1*$^{+/+}$, 6; *Cdh1*$^{GT/+}$, 15; and *Cdh1*$^{GT/GT}$, 10; at 13.5 dpc, *Cdh1*$^{+/-}$, 8; Cdh1$^{GT/+}$, 8; and *Cdh1*$^{GT/GT}$, 10. (C) The eyes of wild-type and *Cdh1*$^{GT/GT}$ mice at 18.5 dpc were obtained from tetraploid complementation. The arrows indicate the margin of the eyelid. (D) Hematoxylin-eosin staining of transverse eye sections from 18.5-dpc embryos, as in panel C. The arrows indicate the margin of the eyelid. (E) Scanning electron micrographs of the eyes of wild-type or *Cdh1*$^{GT/GT}$ rescue embryos at the indicated dpc. The arrowheads indicate eyelid fusion in wild-type embryos. (F) Percentage of embryos with eyelids open at the indicated dpc. The number of embryos analyzed was as follows: at 14.5 dpc, *Cdh1*$^{+/+}$, 2; and *Cdh1*$^{GT/GT}$, 2; at 15.5 dpc, *Cdh1*$^{+/+}$, 8; *Cdh1*$^{GT/GT}$, 5; at 16.5 dpc, *Cdh1*$^{+/+}$, 8; and *Cdh1*$^{GT/GT}$, 3; at 18.5 dpc, *Cdh1*$^{+/+}$, 9; and *Cdh1*$^{GT/GT}$, 10. (G) Immunohistochemical staining of p190 in transverse sections of the eyelid of wild-type and *Cdh1*$^{GT/GT}$ rescue embryos at 18.5 dpc. The arrows indicate the margin of the eyelid. (H) Sagittal sections of rescue embryos at 18.5 dpc were stained with an anti-p190 antibody. The arrows indicate p190 staining in the central nervous system of *Cdh1*$^{GT/GT}$ embryos. Bars, 50 μm (D) and 100 μm (E).

p190, which is a Rho family GTPase-activating protein, has been reported to account for a substantial fraction of the total inhibitory activity of Rho in cultured cells (52). RhoGAPs are regulated by various mechanisms, including protein-protein interactions, phospholipid modification, phosphorylation, subcellular translocation, and proteolytic degradation (7, 30). The Src-mediated phosphorylation of p190 promotes its RhoGAP activity, whereas ROCK-mediated phosphorylation of p190 leads to its inactivation via the inhibition of its binding to Rnd (5, 30). In addition to phosphorylation, our results suggested that control of the abundance of p190 was another regulatory mechanism of its activity (Fig. 6D to G).

p190 expression is not constant throughout the cell cycle (45). p190 expression decreases during late mitosis, and this reduction is dependent on ubiquitin-mediated protein degradation (45). APC/C^{Cdh1} is a strong E3 ubiquitin ligase candidate for p190 as the timing of APC/C^{Cdh1} activation fits well with the timing of p190 degradation. However, this has not been proven previously. In this study, we presented data that support our hypothesis as Cdh1 formed a physical complex with p190. We also found that Cdh1 stimulated the efficient

ubiquitination and degradation of p190, both *in vitro* and *in vivo* (Fig. 5). Su et al. proposed that the reduction of endogenous p190 levels during late mitosis is linked to completion of cytokinesis. Cytokinesis is driven by an actin and myosin contractile ring. Constitutive inhibition and activation of Rho block cytokinesis, which suggests that a complex regulation of Rho activity is required for the process (13). Constitutive overexpression of p190 in breast cancer cells leads to multinucleation, which is often caused by cytokinesis failure and is reminiscent of the phenotype of *Cdh1*-null fibroblasts (15, 45). Therefore, Cdh1 may regulate not only cell motility but also cytokinesis via p190.

p190 has five D boxes and two KEN boxes (Fig. 4A), which are degradation motifs that are recognized by APC/C^{Cdh1} (35). Our mutational analysis indicated that KEN and D boxes within the MD region were relevant for the interaction with Cdh1 (Fig. 4B). Cdh1 effectively stimulated ubiquitination and subsequent degradation of p190 (Fig. 5). However, Cdh1 knockdown did not inhibit the ubiquitination of p190 completely (Fig. 5B and C), which suggests that several other candidate E3 ligases, such as the Skp1-cullin-F-box complex, may also be involved in the process. Thus, our results suggest that APC/C^{Cdh1} is a major, but not exclusive, E3 ligase for p190. Further analysis will be required to explore the exact molecular mechanism of control of p190 abundance.

All Rho isoforms (RhoA, -B, and -C) induce stress fiber formation when overexpressed in fibroblasts (18). *RhoB*-null and *RhoC*-null mice are viable and have no major developmental defects (17, 26). The significance of RhoA in mammalian development is unknown because of a lack of *RhoA* KO mice (18). It is difficult at present to understand the developmental role of Cdh1 in terms of its correlation with Rho as we are unable to compare it with *RhoA* KO mice. Among the various downstream effectors of Rho, ROCKs were the first to be identified and appeared to mediate a significant proportion of the Rho signals (2, 39). Therefore, comparison of $Cdh1^{GT/GT}$ mice with *ROCK*-deficient mice may be useful for the elucidation of the physiological roles of Cdh1. *ROCK* KO mice have been generated, and the involvement of ROCK in the developmental process has been analyzed (44, 49). Most *ROCK* $I^{-/-}$ mice die soon after birth, and homozygous embryos exhibit failed eyelid and ventral wall closure (44). Most *ROCK* $II^{-/-}$ mice also exhibit embryonic lethality after 13.5 dpc and show defects in the placental labyrinth layer, with disruptive architecture and extensive thrombus formation (49). In the present study, the developmental failures observed in $Cdh1^{GT/GT}$ embryos have many similarities with those of both *ROCK* $I^{-/-}$ and *ROCK* $II^{-/-}$ mice. Cdh1 was highly expressed in the labyrinth layer of the placenta, similarly to ROCK II (see Fig. S3 in the supplemental material). A disorganized structure and an increased frequency of thrombus formation were found in the labyrinth layer of $Cdh1^{GT/GT}$ placenta (Fig. 7A and B). Loss of Cdh1 leads to embryonic lethality because of placental insufficiency at midgestation, which happens earlier than in *ROCK*-null embryos (15, 24). One possible reason for these differences in lethal timing is that *ROCK* KO mice have no TGC abnormalities (44, 49). Both the labyrinth and the TGC layer were compromised in *Cdh1*-deficient placentas, which may cause a more severe phenotype than that of *ROCK*-null embryos. We also confirmed the significance of the placenta in $Cdh1^{GT/GT}$ embryonic lethality using tetraploid complementation rescue. This technique allowed $Cdh1^{GT/GT}$ embryos to survive until birth; nevertheless, these embryos showed a delayed timing of eyelid closure compared with that of their normal counterparts. Embryos derived from wild-type ES cell aggregation resulted in delayed eyelid closure compared with those derived from normal pregnancy (44); however, $Cdh1^{GT/GT}$ embryos showed an even slower timing, which seems to rule out the possibility of an effect of the artificial defects of the delay associated with embryonic manipulation (Fig. 7C to F). The p190 mRNA is expressed abundantly in the central nervous system during mouse development (10). We found that the p190 protein was highly expressed in the spinal cord of $Cdh1^{GT/GT}$ embryos (Fig. 7H). Furthermore, the p190 protein also accumulated in epithelial cells of the eyelid of $Cdh1^{GT/GT}$ mice (Fig. 7G), which supports our notion that Cdh1 may modulate the RhoA/ROCK signaling axis via p190 regulation during mouse development.

In summary, our findings provided new insights into the physiological roles of Cdh1. Cdh1 regulated Rho via a major RhoGAP, p190. Therefore, Cdh1 participated not only in cell cycle regulation but also in cell motility. Its functional interaction with Rho provides a broader functional perspective of Cdh1 under physiological and pathological conditions.

ACKNOWLEDGMENTS

We thank H. Sabe for the pEGFP full-length p190 expression vector, P. P. Pandolfi and T. Maeda for the pWZL-hyg-SV40 large T retrovirus vector, T. Shinoda for help in the quantitative analysis of fluorescent intensity, I. Ishimatsu and M. Nakata for technical assistance in the histological analyses, Y. Ito and N. Suzuki for animal maintenance, K. Arai for secretarial assistance, and M. Amano, S. Nakada, and all members of the Saya lab for helpful comments and discussions. We also thank the members of the Gene Technology Center and CARD at Kumamoto University for technical assistance and animal maintenance.

This study was supported by grants from the Ministry of Education, Culture, Sports, Science, and Technology (MEXT) of Japan (to S.K. [20590315 and 20058033] and H.S. [17013070]).

REFERENCES

1. **Almeida, A., J. P. Bolanos, and S. Moreno.** 2005. Cdh1/Hct1-APC is essential for the survival of postmitotic neurons. J. Neurosci. **25**:8115–8121.
2. **Amano, M., Y. Fukata, and K. Kaibuchi.** 2000. Regulation and functions of Rho-associated kinase. Exp. Cell Res. **261**:44–51.
3. **Araki, K., T. Imaizumi, K. Okuyama, Y. Oike, and K. Yamamura.** 1997. Efficiency of recombination by Cre transient expression in embryonic stem cells: comparison of various promoters. J. Biochem. **122**:977–982.
4. **Araki, K., N. Takeda, A. Yoshiki, Y. Obata, N. Nakagata, T. Shiroishi, K. Moriwaki, and K. Yamamura.** 2009. Establishment of germline-competent embryonic stem cell lines from the MSM/Ms strain. Mamm. Genome **20**:14–20.
5. **Arthur, W. T., L. A. Petch, and K. Burridge.** 2000. Integrin engagement suppresses RhoA activity via a c-Src-dependent mechanism. Curr. Biol. **10**:719–722.
6. **Bashir, T., N. V. Dorrello, V. Amador, D. Guardavaccaro, and M. Pagano.** 2004. Control of the SCF(Skp2-Cks1) ubiquitin ligase by the APC/C^{Cdh1} ubiquitin ligase. Nature **428**:190–193.
7. **Bernards, A., and J. Settleman.** 2004. GAP control: regulating the regulators of small GTPases. Trends Cell Biol. **14**:377–385.
8. **Bernards, A., and J. Settleman.** 2005. GAPs in growth factor signalling. Growth Factors **23**:143–149.
9. **Brandeis, M., and T. Hunt.** 1996. The proteolysis of mitotic cyclins in mammalian cells persists from the end of mitosis until the onset of S phase. EMBO J. **15**:5280–5289.
10. **Brouns, M. R., S. F. Matheson, K. Q. Hu, I. Delalle, V. S. Caviness, J. Silver, R. T. Bronson, and J. Settleman.** 2000. The adhesion signaling molecule p190 RhoGAP is required for morphogenetic processes in neural development. Development **127**:4891–4903.
11. **Clark, E. A., and J. S. Brugge.** 1995. Integrins and signal transduction pathways: the road taken. Science **268**:233–239.

12. **Di Fiore, B., and J. Pines.** 2007. Emi1 is needed to couple DNA replication with mitosis but does not regulate activation of the mitotic APC/C. J. Cell Biol. **177:**425–437.
13. **Etienne-Manneville, S., and A. Hall.** 2002. Rho GTPases in cell biology. Nature **420:**629–635.
14. **Findlater, G. S., R. D. McDougall, and M. H. Kaufman.** 1993. Eyelid development, fusion and subsequent reopening in the mouse. J. Anat. **183:**121–129.
15. **Garcia-Higuera, I., E. Manchado, P. Dubus, M. Canamero, J. Mendez, S. Moreno, and M. Malumbres.** 2008. Genomic stability and tumour suppression by the APC/C cofactor Cdh1. Nat. Cell Biol. **10:**802–811.
16. **Gieffers, C., B. H. Peters, E. R. Kramer, C. G. Dotti, and J. M. Peters.** 1999. Expression of the CDH1-associated form of the anaphase-promoting complex in postmitotic neurons. Proc. Natl. Acad. Sci. U. S. A. **96:**11317–11322.
17. **Hakem, A., O. Sanchez-Sweatman, A. You-Ten, G. Duncan, A. Wakeham, R. Khokha, and T. W. Mak.** 2005. RhoC is dispensable for embryogenesis and tumor initiation but essential for metastasis. Genes Dev. **19:**1974–1979.
18. **Heasman, S. J., and A. J. Ridley.** 2008. Mammalian Rho GTPases: new insights into their functions from in vivo studies. Nat. Rev. Mol. Cell Biol. **9:**690–701.
19. **King, R. W., J. M. Peters, S. Tugendreich, M. Rolfe, P. Hieter, and M. W. Kirschner.** 1995. A 20S complex containing CDC27 and CDC16 catalyzes the mitosis-specific conjugation of ubiquitin to cyclin B. Cell **81:**279–288.
20. **Konishi, Y., J. Stegmuller, T. Matsuda, S. Bonni, and A. Bonni.** 2004. Cdh1-APC controls axonal growth and patterning in the mammalian brain. Science **303:**1026–1030.
21. **Kotani, S., S. Tugendreich, M. Fujii, P. M. Jorgensen, N. Watanabe, C. Hoog, P. Hieter, and K. Todokoro.** 1998. PKA and MPF-activated Polo-like kinase regulate anaphase-promoting complex activity and mitosis progression. Mol. Cell **1:**371–380.
22. **Kraft, C., M. Gmachl, and J. M. Peters.** 2006. Methods to measure ubiquitin-dependent proteolysis mediated by the anaphase-promoting complex. Methods **38:**39–51.
23. **Kuninaka, S., M. Nomura, T. Hirota, S. Iida, T. Hara, S. Honda, N. Kunitoku, T. Sasayama, Y. Arima, T. Marumoto, K. Koja, S. Yonehara, and H. Saya.** 2005. The tumor suppressor WARTS activates the Omi/HtrA2-dependent pathway of cell death. Oncogene **24:**5287–5298.
24. **Li, M., Y.-H. Shin, L. Hou, X. Huang, Z. Wei, E. Klann, and P. Zhang.** 2008. The adaptor protein of the anaphase promoting complex Cdh1 is essential in maintaining replicative lifespan and in learning and memory. Nat. Cell Biol. **10:**1083–1089.
25. **Li, W., G. Wu, and Y. Wan.** 2007. The dual effects of Cdh1/APC in myogenesis. FASEB J. **21:**3606–3617.
26. **Liu, A. X., N. Rane, J. P. Liu, and G. C. Prendergast.** 2001. RhoB is dispensable for mouse development, but it modifies susceptibility to tumor formation as well as cell adhesion and growth factor signaling in transformed cells. Mol. Cell. Biol. **21:**6906–6912.
27. **Machida, Y. J., and A. Dutta.** 2007. The APC/C inhibitor, Emi1, is essential for prevention of rereplication. Genes Dev. **21:**184–194.
28. **Maeda, T., R. M. Hobbs, T. Merghoub, I. Guernah, A. Zelent, C. Cordon-Cardo, J. Teruya-Feldstein, and P. P. Pandolfi.** 2005. Role of the proto-oncogene Pokemon in cellular transformation and ARF repression. Nature **433:**278–285.
29. **Mitsunaga, K., K. Araki, H. Mizusaki, K.-i. Morohashi, K. Haruna, N. Nakagata, V. Giguère, K.-i. Yamamura, and K. Abe.** 2004. Loss of PGC-specific expression of the orphan nuclear receptor ERR-β results in reduction of germ cell number in mouse embryos. Mech. Dev. **121:**237–246.
30. **Mori, K., M. Amano, M. Takefuji, K. Kato, Y. Morita, T. Nishioka, Y. Matsuura, T. Murohara, and K. Kaibuchi.** 2009. Rho-kinase contributes to sustained RhoA activation through phosphorylation of p190A RhoGAP. J. Biol. Chem. **284:**5067–5076.
31. **Nagy, A.** 2003. Manipulating the mouse embryo: a laboratory manual, 3rd ed. Cold Spring Harbor Laboratory Press, Cold Spring Harbor, NY.
32. **Narumiya, S., M. Tanji, and T. Ishizaki.** 2009. Rho signaling, ROCK and mDia1, in transformation, metastasis and invasion. Cancer Metastasis Rev. **28:**65–76.
33. **Olofsson, B.** 1999. Rho guanine dissociation inhibitors: pivotal molecules in cellular signalling. Cell Signal **11:**545–554.
34. **Papaioannou, V. E., and R. Behringer.** 2005. Mouse phenotypes: a handbook of mutation analysis. Cold Spring Harbor Laboratory Press, Cold Spring Harbor, NY.
35. **Peters, J. M.** 2006. The anaphase promoting complex/cyclosome: a machine designed to destroy. Nat. Rev. Mol. Cell Biol. **7:**644–656.
36. **Reid, T., T. Furuyashiki, T. Ishizaki, G. Watanabe, N. Watanabe, K. Fujisawa, N. Morii, P. Madaule, and S. Narumiya.** 1996. Rhotekin, a new putative target for Rho bearing homology to a serine/threonine kinase, PKN, and rhophilin in the Rho-binding domain. J. Biol. Chem. **271:**13556–13560.
37. **Ren, X. D., W. B. Kiosses, and M. A. Schwartz.** 1999. Regulation of the small GTP-binding protein Rho by cell adhesion and the cytoskeleton. EMBO J. **18:**578–585.
38. **Ridley, A. J., and A. Hall.** 1992. The small GTP-binding protein rho regulates the assembly of focal adhesions and actin stress fibers in response to growth factors. Cell **70:**389–399.
39. **Riento, K., and A. J. Ridley.** 2003. Rocks: multifunctional kinases in cell behaviour. Nat. Rev. Mol. Cell Biol. **4:**446–456.
40. **Sahai, E., R. García-Medina, J. Pouyssegur, and E. Vial.** 2007. Smurf1 regulates tumor cell plasticity and motility through degradation of RhoA leading to localized inhibition of contractility. J. Cell Biol. **176:**35–42.
41. **Schmidt, A., and A. Hall.** 2002. Guanine nucleotide exchange factors for Rho GTPases: turning on the switch. Genes Dev. **16:**1587–1609.
42. **Schoenwaelder, S. M., and K. Burridge.** 1999. Bidirectional signaling between the cytoskeleton and integrins. Curr. Opin. Cell Biol. **11:**274–286.
43. **Schwab, M., A. S. Lutum, and W. Seufert.** 1997. Yeast Hct1 is a regulator of Clb2 cyclin proteolysis. Cell **90:**683–693.
44. **Shimizu, Y., D. Thumkeo, J. Keel, T. Ishizaki, H. Oshima, M. Oshima, Y. Noda, F. Matsumura, M. M. Taketo, and S. Narumiya.** 2005. ROCK-I regulates closure of the eyelids and ventral body wall by inducing assembly of actomyosin bundles. J. Cell Biol. **168:**941–953.
45. **Su, L., J. M. Agati, and S. J. Parsons.** 2003. p190RhoGAP is cell cycle regulated and affects cytokinesis. J. Cell Biol. **163:**571–582.
46. **Sudakin, V., D. Ganoth, A. Dahan, H. Heller, J. Hershko, F. C. Luca, J. V. Ruderman, and A. Hershko.** 1995. The cyclosome, a large complex containing cyclin-selective ubiquitin ligase activity, targets cyclins for destruction at the end of mitosis. Mol. Biol. Cell **6:**185–197.
47. **Sudo, T., Y. Ota, S. Kotani, M. Nakao, Y. Takami, S. Takeda, and H. Saya.** 2001. Activation of Cdh1-dependent APC is required for G1 cell cycle arrest and DNA damage-induced G2 checkpoint in vertebrate cells. EMBO J. **20:**6499–6508.
48. **Taniwaki, T., K. Haruna, H. Nakamura, T. Sekimoto, Y. Oike, T. Imaizumi, F. Saito, M. Muta, Y. Soejima, A. Utoh, N. Nakagata, M. Araki, K. Yamamura, and K. Araki.** 2005. Characterization of an exchangeable gene trap using pU-17 carrying a stop codon-beta geo cassette. Dev. Growth Differ. **47:**163–172.
49. **Thumkeo, D., J. Keel, T. Ishizaki, M. Hirose, K. Nonomura, H. Oshima, M. Oshima, M. M. Taketo, and S. Narumiya.** 2003. Targeted disruption of the mouse Rho-associated kinase 2 gene results in intrauterine growth retardation and fetal death. Mol. Cell. Biol. **23:**5043–5055.
50. **Totsukawa, G., Y. Yamakita, S. Yamashiro, D. J. Hartshorne, Y. Sasaki, and F. Matsumura.** 2000. Distinct roles of Rock (Rho-Kinase) and Mlck in spatial regulation of Mlc phosphorylation for assembly of stress fibers and focal adhesions in 3t3 fibroblasts. J. Cell Biol. **150:**797–806.
51. **Tsubouchi, A., J. Sakakura, R. Yagi, Y. Mazaki, E. Schaefer, H. Yano, and H. Sabe.** 2002. Localized suppression of RhoA activity by Tyr31/118-phosphorylated paxillin in cell adhesion and migration. J. Cell Biol. **159:**673–683.
52. **Vincent, S., and J. Settleman.** 1999. Inhibition of RhoGAP activity is sufficient for the induction of Rho-mediated actin reorganization. Eur. J. Cell Biol. **78:**539–548.
53. **Visintin, R., S. Prinz, and A. Amon.** 1997. CDC20 and CDH1: A family of substrate-specific activators of APC-dependent proteolysis. Science **278:**460–463.
54. **Wan, Y., X. Liu, and M. W. Kirschner.** 2001. The anaphase-promoting complex mediates TGF-beta signaling by targeting SnoN for destruction. Mol. Cell **8:**1027–1039.
55. **Wang, H. R., Y. Zhang, B. Ozdamar, A. A. Ogunjimi, E. Alexandrova, G. H. Thomsen, and J. L. Wrana.** 2003. Regulation of cell polarity and protrusion formation by targeting RhoA for degradation. Science **302:**1775–1779.
56. **Wei, W., N. G. Ayad, Y. Wan, G. J. Zhang, M. W. Kirschner, and W. G. Kaelin, Jr.** 2004. Degradation of the SCF component Skp2 in cell-cycle phase G1 by the anaphase-promoting complex. Nature **428:**194–198.
57. **Yagi, T., T. Tokunaga, Y. Furuta, S. Nada, M. Yoshida, T. Tsukada, Y. Saga, N. Takeda, Y. Ikawa, and S. Aizawa.** 1993. A novel ES cell line, TT2, with high germline-differentiating potency. Anal. Biochem. **214:**70–76.
58. **Yamana, N., Y. Arakawa, T. Nishino, K. Kurokawa, M. Tanji, R. E. Itoh, J. Monypenny, T. Ishizaki, H. Bito, K. Nozaki, N. Hashimoto, M. Matsuda, and S. Narumiya.** 2006. The Rho-mDia1 pathway regulates cell polarity and focal adhesion turnover in migrating cells through mobilizing Apc and c-Src. Mol. Cell. Biol. **26:**6844–6858.

Clin J Gastroenterol (2010) 3:271–278
DOI 10.1007/s12328-010-0177-6

CLINICAL REVIEW

Insulin resistance and hepatocarcinogenesis

Yutaka Sasaki

Received: 18 August 2010 / Accepted: 20 August 2010 / Published online: 29 September 2010

Abstract Hepatocellular carcinoma (HCC) accounts for 85–90% of liver cancers and is one of the most frequent carcinomas in the world. HCCs classically develop against the background of chronic liver diseases. Common causes of such liver diseases are viral hepatitis, alcoholic hepatitis, or immune-related diseases; however, 15–50% of patients with HCCs have none of these classic antecedents, especially in developed countries. In this context, obesity and diabetes mellitus have been found to exhibit an increased risk of HCC. Both conditions are associated with insulin resistance. The tumorigenic effects of insulin resistance and complementary hyperinsulinemia could be mediated directly by insulin signaling, or indirectly related to changes in endogeneous hormone metabolism, particularly insulin-like growth factor I. Conversely, insulin resistance may be a consequence of obesity and hepatic inflammation, both of which can themselves promote tumorigenesis, mainly through cytokine production and/or generation of oxidative stress. Because the prevalence of obesity is now increasing throughout the world, insulin resistance is sure to be emphasized as a major factor in hepatocarcinogenesis in the foreseeable future.

Keywords Insulin resistance · Obesity · Insulin · IGF-1 · Oxidative stress · HCC

Introduction

Primary liver cancer is the fifth most common malignancy worldwide, and the third leading cause of cancer-related death, exceeded only by lung and stomach cancer [1]. Hepatocellular carcinoma (HCC) accounts for 85–90% of these primary liver cancers. The estimated incidence of new cases is approximately 0.5–1 million per year, causing 0.6 million deaths annually worldwide [2]. Importantly, a difference of HCC burden has been noted among countries and/or regions; more than 80% of HCC cases occur in developing countries, particularly in Africa or Eastern Asia, with China alone providing more than 50% of cases worldwide.

The incidence of HCC in these areas is now decreasing, but has recently started to rise in developed countries. There has been an increase of about 80% in the annual incidence during the past two decades in the United States [3].

HCCs develop against the background of chronic liver diseases. Common causes of such diseases are viral hepatitis (HBV or HCV), alcoholic hepatitis, or immune-related diseases (primary biliary cirrhosis and autoimmune hepatitis); however, 15–50% of patients with HCCs have none of these classic antecedents, especially in developed countries [2].

Emerging evidence suggests an association between metabolic factors and risk of HCC in developed countries. In this context, the prevalence of obesity has been increasing rapidly in the world. Epidemiologic studies clearly indicate an association between obesity and the development of a variety of cancers, although the mechanisms whereby obesity induces or promotes tumorigenesis vary among cancers. Obesity and diabetes mellitus have been found to be associated with an increased risk of HCC in several epidemiologic studies. Large population studies have reported that obesity increases the risk of development and death due to HCC by 2–5 times [4–8].

Y. Sasaki (✉)
Department of Gastroenterology and Hepatology,
Graduate School of Medical Sciences, Kumamoto University,
1-1-1 Honjo, Kumamoto, Kumamoto 860-8556, Japan
e-mail: sasakiy@kumamoto-u.ac.jp

In addition, a number of case–control and cohort studies have linked diabetes to a two-fold increased risk of HCC [9–12].

With the increasing prevalence of obesity and diabetes, it is important to explain the complex relationship between these 2 factors as well as other metabolic factors and the risk of HCC.

Obesity and insulin resistance

It has been clarified that adipose tissue constitutes an endocrine and metabolic organ that can exert a wide range of physiologic effects [13]. In response to signals from other tissues, adipose tissue responds by an increase or decrease in the release of free fatty acid (FFA). In addition, adipose tissue is involved in energy balance and lipid metabolism in terms of releasing adipocytokines. Obesity is associated with an increased release of FFA and multiple pro-inflammatory cytokines including tumor necrosis factor alpha (TNFα), leptin, interleukin (IL)-6, resistin, reduced release of adiponectin (an anti-inflammatory polypeptide from adipose tissue), which gives rise to insulin resistance. These processes will develop into hepatic steatosis and inflammation in the liver [14].

Insulin resistance is defined as a situation of reduced sensitivity to insulin in insulin-responsive tissues, and its main consequences include an impaired ability of insulin to suppress hepatic glucose production and stimulate peripheral glucose elimination. Providing that β-cell function is preserved, insulin secretion increases to overcome insulin resistance, and glucose levels are normalized. Thus, the resulting compensatory hyperinsulinemia is a hallmark of insulin resistance. Chronic hyperinsulinemia has been associated with a variety of cancers [15–19]. Evidence has emerged that chronic insulin therapy significantly increases the risk of colorectal cancer among type 2 diabetes mellitus patients. In addition, cancer risk increases with the increasing duration of insulin therapy [20]. These clinical observations highlight the potential importance of insulin as a cancer risk factor.

It is important to note that promotion of cancer by insulin resistance needs to be differentiated from the promotion of cancer by the conditions that coincidently induce insulin resistance.

How does insulin resistance participate in hepatocarcinogenesis?

The tumorigenic effects of insulin resistance could be mediated directly by insulin signaling, or indirectly related to changes in endogeneous hormone metabolism, secondary to hyperinsulinemia.

Direct action of insulin on growth promotion via classical insulin signaling

Insulin exerts its action upon binding to its specific receptor with tyrosine kinase activity. In turn, the activated insulin receptor promotes the phosphorylation of insulin receptor substrate-1 (IRS-1) and transmission of the insulin signal through two major phosphorylation cascades: phosphoinositide 3-kinase (PI3K) and mitogen-activated protein kinase (MAPK) cascades (Fig. 1). PI3K cascade induces translocation of the serine/threonine protein kinase Akt, from cytoplasm to the cell membrane, where Akt stimulates the phosphorylation and consequent inhibition or activation of a variety of proteins involving cell growth, division, and survival, as well as lipid and carbohydrate metabolisms, e.g. the pro-apoptotic Bcl-2 family member BAD and the growth-related mTOR.

The role of PI3K cascade for cell proliferation and survival has been clarified by a high prevalence in a variety of cancers with a loss-of-function of phosphatase and tensin homolog deleted on chromosome 10 (PTEN), which enhances PI3K cascade [21].

Phosphorylated IRS-1 can also mediate the formation of a complex between the adaptor protein growth factor receptor-bound protein 2 (Grb2) and the guanine nucleotide-exchange factor mammalian Son of sevenless (mSos). The Grb2–mSos complex can then activate p21Ras. In turn, activated p21Ras induces the activation of the MAPK cascade, leading to the activation of transcription factors involved in cell proliferation. The importance of the Ras/MAPK cascade for cell proliferation is supported by the finding that the prevalence of p21Ras over-expression has been reported to be high in a variety of cancers [22].

Although in vitro studies show that insulin can promote cell proliferation, supra-physiological insulin concentrations have been used in these studies. Thus, it remains obscure whether insulin can exert any growth-promoting effect or not.

Insulin can, however, induce other changes to amplify growth-promoting properties. In this regard, chronic hyperinsulinemia increases the intracellular content of farnesylated p21Ras and loading of p21Ras with guanosine triphosphate, which may amplify growth factor signaling through the MAPK cascade [23].

Hepatocarcinogenesis is a multi-factorial, multi-stage process, and one of these stages can include over-expression of insulin signal components. In this context, IRS-1 has been shown to be up-regulated in HCC [24, 25]. Thus, the compensatory hyperinsulinemia in insulin resistance might provide an additional stimulation to cell proliferation and survival in the conditions where insulin signaling has